One-Dimensional Activation and Radiological Dose Calculations for the Light Ion Fusion Target Development Facility

D.L. Henderson, G.A. Moses and R.R. Peterson

October 1985

UWFDM-636

FUSION TECHNOLOGY INSTITUTE

UNIVERSITY OF WISCONSIN

MADISON WISCONSIN

One-Dimensional Activation and Radiological Dose Calculations for the Light Ion Fusion Target Development Facility

D.L. Henderson, G.A. Moses and R.R. Peterson

Fusion Technology Institute
University of Wisconsin
1500 Engineering Drive
Madison, WI 53706

http://fti.neep.wisc.edu

October 1985

UWFDM-636

ONE-DIMENSIONAL ACTIVATION AND RADIOLOGICAL DOSE CALCULATIONS FOR THE LIGHT ION FUSION TARGET DEVELOPMENT FACILITY

D.L. Henderson

G.A. Moses

R.R. Peterson

Fusion Technology Institute
1500 Johnson Drive
University of Wisconsin-Madison
Madison, Wisconsin 53706

October 1985

UWFDM-636

TABLE OF CONTENTS

ABSTRACT

Radioactivity and biological dose calculations have been performed for the target chamber of the Target Development Facility (TDF). Two conventional shield designs are considered. One has the target chamber submerged 3 m from the surface of a borated water pool, the other has the chamber surrounded by approximately 250 cm of concrete. The first wall materials, Al-6061-T6 and 2-1/4 Cr-1 Mo steel and the ion beam targets, one made from BeO and W and the other from CH_2 and Au, are investigated. Shielding designs are presented that reduce the dose from each of these choices of shield, first wall and target material to acceptable levels. Another option examined to lower the biological dose rates is the placement of an ISSEC (Internal Spectral Shifter and Energy Converter) structure in the interior of the target chamber for the moderation of the high energy neutrons. Two ISSEC materials are considered, one made of H-451 graphite and the other of titanium hydride. Maintenance schedules are presented that are based on the allowable average dose of 1.25 rem per quarter and the graphite ISSEC-aluminum chamber wall computations.

1. INTRODUCTION

The light ion beam fusion target development facility (TDF) is an experimental facility proposed to verify the feasibility of using light ion beams to initiate thermonuclear burn within fusion targets. It is intended to test approximately ten to twelve 50-800 MJ fusion targets per day over a period of five years (~ 15,000 shots over its lifetime). This large number of high yield shots makes the TDF one of the first inertial confinement fusion experiments where radioactivity induced by fusion neutrons could represent a significant biological hazard which would require some form of radiation shield. Therefore, the preliminary design of the facility has the target explosion chamber submerged in a borated water pool below the operating floor as shown in Fig. 1. Because the water shield might be lowered for periodic maintenance either in the chamber's interior or exterior and because workers performing this maintenance may be required to come in close contact with the first wall, it is important to determine the biological doses the workers would be receiving near the target chamber.

As an alternative to the borated water pool shield a design where the target chamber has been enclosed within concrete as shown in Fig. 2 has been investigated. Also, the use of an ISSEC (Internal Spectral Shifter and Energy Converter) structure placed in the interior of the target chamber for the moderation of the high energy neutrons has been examined. Two ISSEC materials, H-451 graphite and titanium hydride, were considered. Calculations of radioactivity induced in Al-6061-T6 and 2-1/4 Cr-1 Mo steel walls and in fusion targets, one made from BeO and W and the other from CH_2 and Au, have been done. The resultant biological dose of the accumulated radioactive target debris and first wall structure has been computed. These results repre-

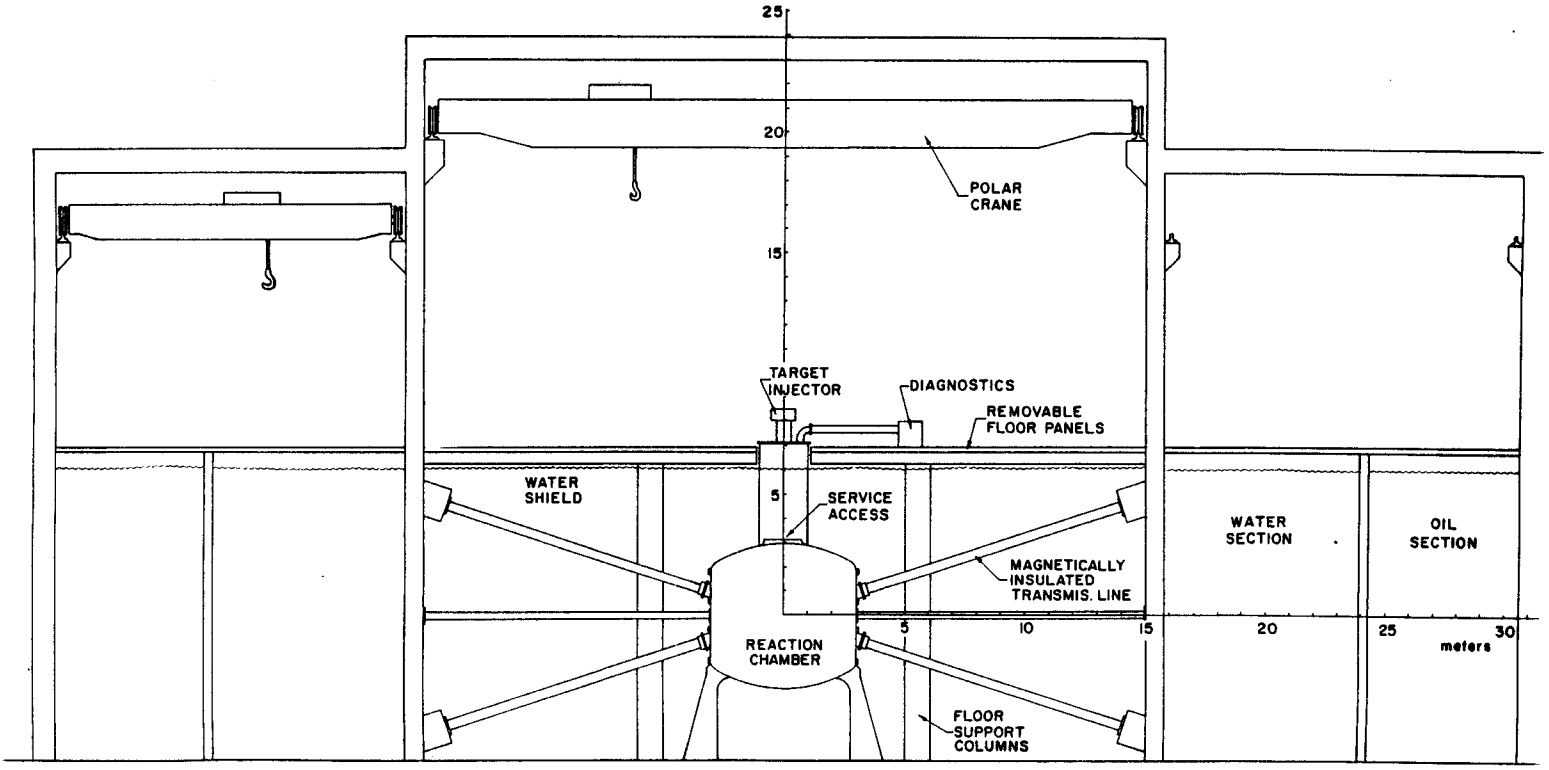

Fig. 1. Preliminary design of the Light Ion Fusion Target Development Facility.

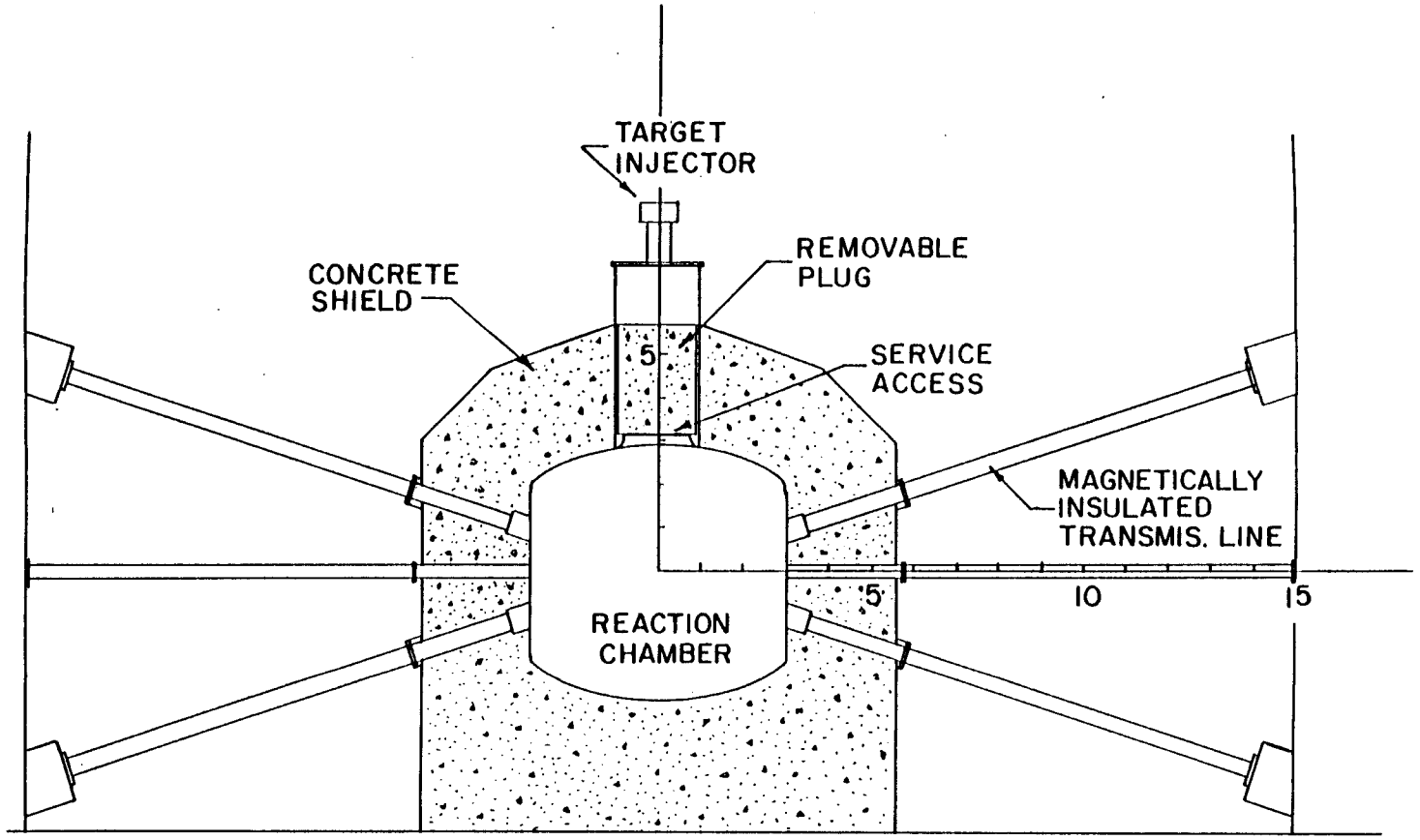

Fig. 2. Alternative design: target chamber enclosed within a concrete shield.

sent improvements on early calculations[1] which did not consider the effects of the activated target debris and which contained some inaccuracies in the first wall dose rate results.

Section 2 contains a brief description of the codes and data libraries employed for the calculations and of the calculational model used for the target and chamber wall computations. In addition, the calculational schemes used to compute the dose rate for the facility are outlined in this section. Section 3 contains the results of the target activation analysis, target and chamber wall dose rate computations and the ISSEC and chamber wall dose rate calculations. Also contained therein is an outline of the maintenance schedule for the facility and a brief discussion of some peculiarities associated with the pulsed nature of the facility. A brief summary of the results is then given in Section 4.

2. METHOD OF SOLUTION

2.1. Target Design

For the radioactive target debris analysis, two ion beam targets are considered. Both are based upon a target design published by Bangerter and Meeker[2] (see Fig. 3). The targets are composed of a 1 mg DT region surrounded by a BeO pusher and a W tamper or a CH_2 pusher with a Au tamper. The mass of material contained in each zone is given in Table 1 and the nuclide densities in Table 2. The compressed target configuration used for the neutron transport and neutron activation calculations is shown in Fig. 4. A fuel burnup fraction of 30% was assumed giving approximately 100 MJ of released fusion energy with 71 MJ of that being in neutrons.

For a comparison between target debris dose rates and the first wall material doses, the radioactive target debris from each pulse during a 1 year

Table 1. Target Constituents and Their Masses

Region	Target 1 Comp.	Target 1 Mass	Target 2 Comp.	Target 2 Mass
1	DT	1 mg	DT	1 mg
2	CH_2	2.36 mg	BeO	2.36 mg
3	CH_2	14.42 mg	BeO	14.42 mg
4	Au	123.32 mg	W	122.55 mg

Table 2. Nuclide Densities of Target Constituents

Region	Target 1 Isotope	Target 1 Density [atoms/b-cm]	Target 2 Isotope	Target 2 Density [atoms/b-cm]
1	D	22.225	D	22.225
	T	22.225	T	22.225
2	C	7.860	Be	4.409
	H	15.720	^{16}O	4.398
			^{17}O	1.675×10^{-3}
			^{18}O	8.993×10^{-3}
3	C	1.322×10^{-2}	Be	7.417×10^{-3}
	H	2.644×10^{-2}	^{16}O	7.399×10^{-3}
			^{17}O	2.819×10^{-6}
			^{18}O	1.513×10^{-5}
4	^{197}Au	5.908×10^{-3}	^{180}W	8.177×10^{-6}
			^{182}W	1.654×10^{-3}
			^{183}W	8.944×10^{-4}
			^{184}W	1.929×10^{-3}
			^{186}W	1.799×10^{-3}

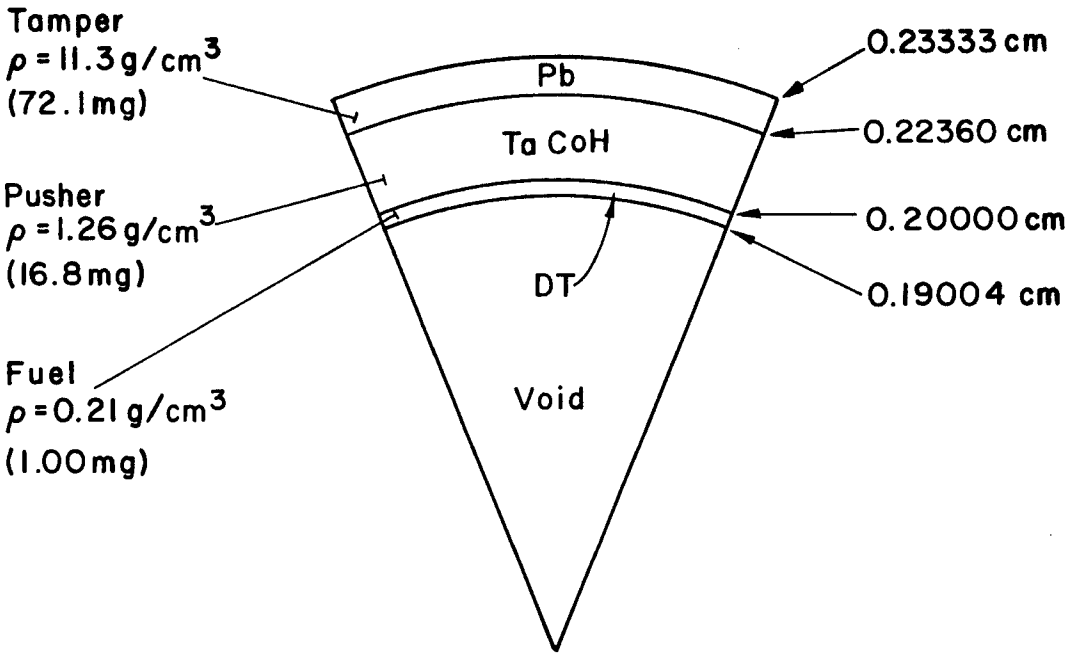

Fig. 3. Reference ion beam target as depicted in Ref. 2.

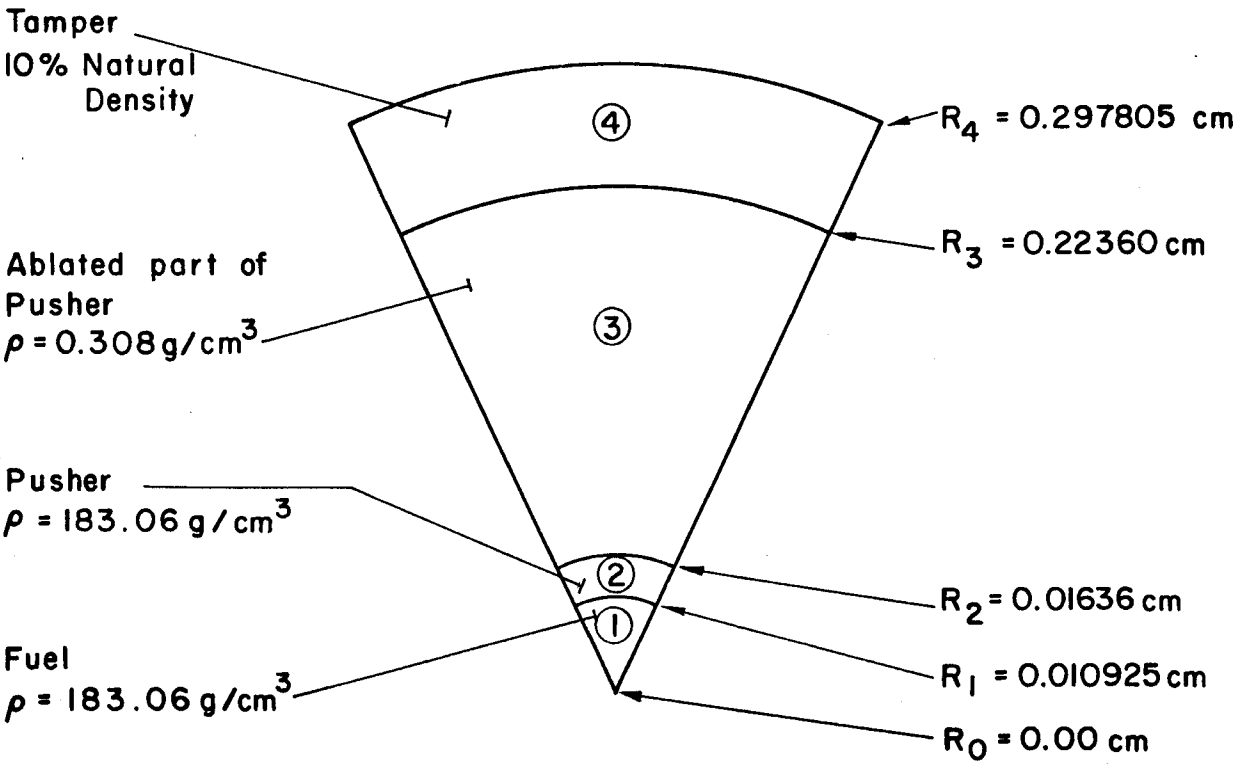

Fig. 4. The compressed target configuration used for the target neutronic and radioactivity calculations.

operation span is accumulated onto the interior surface of the first wall. The radioactivity decay between each pulse and accumulation of the debris is computed by a small computer code which treats the target debris radioactivity produced by each pulse as a delta function in time. The pulse sequence is assumed to be 12 shots per day for 5 days per week for 52 weeks per year which amounts to 3120 shots per year.

2.2. Chamber Wall Design

The neutrons emanating from the target are considered as sources for the first wall neutron transport calculation with the energy spectrum of the fusion neutrons shown in Fig. 5. The energy spectrum consists of a large peak at 14.1 MeV due to the uncollided flux of neutrons escaping the ignited target. This amounts to 70.75% of the released neutrons. There is also some local peaking of the energy spectrum at 2 and 4 MeV caused by backward elastic scattering of 14.1 MeV neutrons with deuterium and tritium. The low energy continuum spectrum consists of neutrons scattered elastically and inelastically within the target and of neutrons produced from (n,2n) and (n,3n) reactions. For additional information on the determination and shape of the spectrum, consult Refs. 3 and 4.

The cylindrically shaped target chamber is approximated by spherical geometry and hence the results represent conditions at the midplane of the chamber. The target chamber has an inner radius of 3.0 meters while the first wall is 3.5 cm thick for ferritic steel and 14.8 cm thick for aluminum. The first wall thickness has been determined through fatigue lifetime analysis.[5] A 3.0 m thick water shield having a boron content of 2000 wppm is assumed for the water pool design. A schematic of the target chamber with the aluminum first wall and borated water shield is displayed in Fig. 6. The alternative

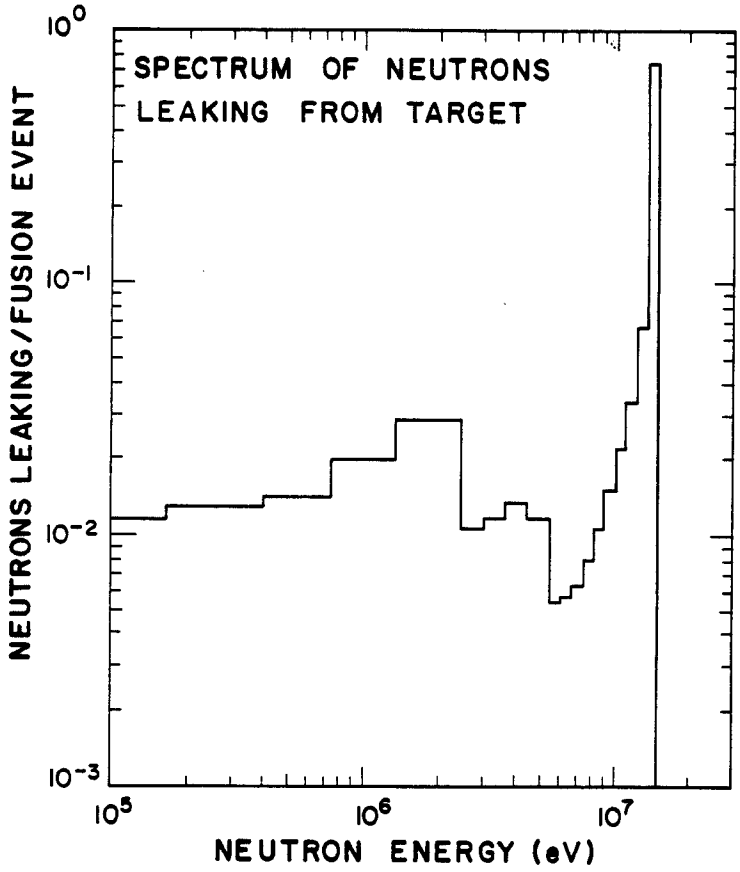

Fig. 5. The spectrum of neutrons leaking from the ion beam target normalized to one fusion neutron.

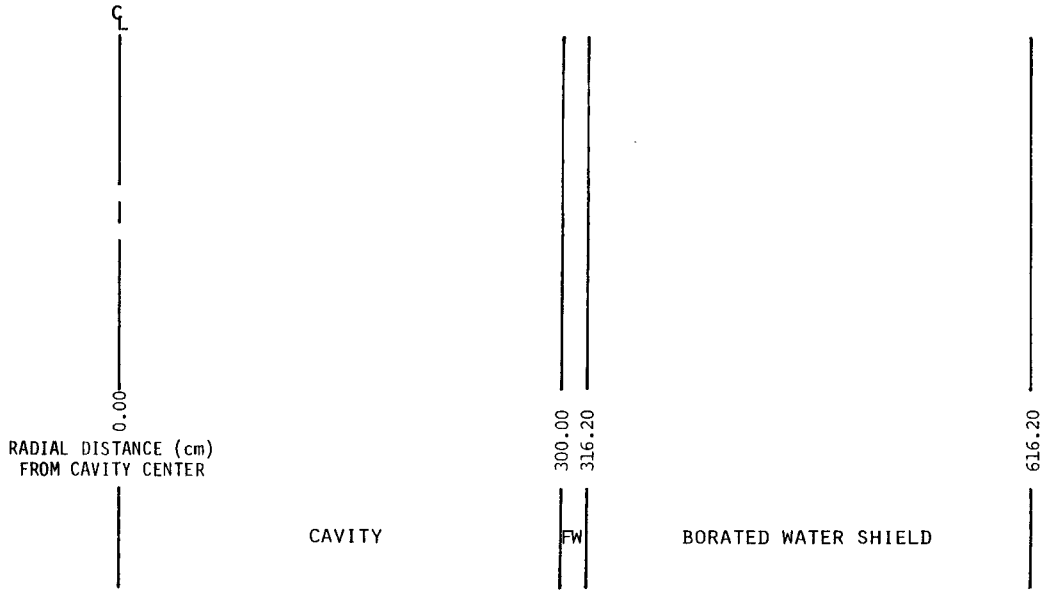

COMPOSITION KEY

F.W*: Aluminum-6061-T6
SHIELD: Water + 2000 wppm Boron

*Note: The chamber wall thickness used for the computations is calculated as follows: the wall thickness , 314.80 cm, plus 10% additional material mass for structural support of the wall. The result is chamber wall thickness of 316.20 cm.

Fig. 6. One-dimensional schematic of the Target Development Facility aluminum chamber and borated water shield used for the neutronic and activation calculations.

design has the target chamber enclosed by a concrete shield containing a boron frites-barytes concrete,[6] 95% vol., and a carbon steel (C1020), 5% vol., as concrete reinforcement. The materials examined for the ISSEC structures are graphite H-451 and titanium hydride (TiH_2). The primary ISSEC design is a 1 meter thick, 40% porosity graphite structure. The thickness of the TiH_2 ISSEC structure is chosen such that the mass of the TiH_2 structure is equivalent to that of the 40% porosity graphite structure. Since TiH_2 is a powder, we choose to can the powder in the same material as the chamber wall (aluminum or steel). For the ISSEC designs, Boral[7] sheets (a B_4C-Al mixture and efficient thermal neutron absorber) are placed on either side of the chamber wall. Schematics of the aluminum chamber with the ISSEC structures, boral sheets and borated water shield are displayed in Figs. 7 and 8.

Since the DKR radioactivity code is a continuous irradiation code, the chamber wall dose rates are computed using an average steady state neutron irradiation flux. The average flux is obtained by averaging the total number of neutrons in the 3120 shots per year over the one year operation period. Thus the dose rate values given assume a continuous one year irradiation of the chamber.

The compositions of the ferritic steel and aluminum walls in weight percent are listed in Table 3 with densities given in Table 4. Impurities contained in the chamber wall materials and included in the activation calculations are listed in Table 5. The compositions of the concrete shield and reinforcing carbon steel are presented in Table 6. Table 7 lists the concrete and borated water shield densities used in the transport and activation calculations. The compositions of the graphite and TiH_2 ISSEC structures and boral sheets in weight percent are listed in Table 8 with densities given in

Table 3. Composition of Chamber Wall Materials

Element [wt.%]	Chamber Wall Material	
	2-1/4 Cr-1 Mo Steel density: 7.82 g/cm^3	Aluminum-6061-T6 density: 2.7 g/cm^3
C	0.11	---
Mg	---	1.0
Al	---	96.55
Si	0.40	0.60
P	0.02	---
S	0.02	---
Ti	0.03	0.15
V	0.03	---
Cr	2.2	0.30
Mn	0.50	0.15
Fe	95.5	0.70
Cu	0.2	0.30
Zn	---	0.25
Mo	1.00	---

Table 4. Chamber Wall Constituent Densities

2-1/4 Cr-1 Mo Steel		Aluminum-6061-T6	
Element	Density [atoms/b-cm]	Element	Density [atoms/b-cm]
C	4.3135×10^{-4}	Mg	6.6889×10^{-4}
Si	6.7080×10^{-4}	Al	5.8192×10^{-2}
P	3.0413×10^{-5}	Si	3.4741×10^{-4}
S	2.9379×10^{-5}	Ti	5.0925×10^{-5}
Ti	2.9499×10^{-5}	Cr	9.3827×10^{-5}
V	2.7737×10^{-5}	Mn	4.4401×10^{-5}
Cr	1.9928×10^{-3}	Fe	2.0383×10^{-4}
Mn	4.2866×10^{-4}	Cu	7.6781×10^{-5}
Fe	8.0452×10^{-2}	Zn	6.2193×10^{-5}
Cu	1.4825×10^{-4}		
Mo	4.9093×10^{-4}		

Table 5. Trace Elements (Ref. 8)

Trace Element (in wppm)	Chamber Material Element		
	Fe	Cr	Mn
Nb	1	---	---
Mo	3	0.4	0.4
Ni	60	3	---
K	4	1	4
Cu	10	---	0.9
Ba	2	---	---

Table 6. Composition of Concrete and Reinforcing Steel

Element [wt.%]	Material	
	Concrete density: 3.1 g/cm^3	Carbon Steel (C1020) density: 7.93 g/cm^3
H	0.56	---
B	1.04	---
C	---	0.20
O	33.80	---
F	0.23	---
Na	1.21	---
Mg	0.23	---
Al	0.64	---
Si	3.31	0.25
S	9.15	---
K	0.10	---
Ca	6.26	---
Mn	0.02	0.45
Fe	2.19	99.10
Zn	0.66	---
Ba	40.13	---

Table 7. Concrete and Borated Water Shield Constituent Densities

Element or Isotope	95 vol.% Concrete + 5 Vol.% Carbon-Steel Density [atoms/b-cm]	2000 wppm Borated Water Density [atoms/b-cm]
H	9.8553×10^{-3}	6.6865×10^{-2}
^{10}B	3.4130×10^{-4}	2.2284×10^{-5}
^{11}B	1.3652×10^{-3}	8.9136×10^{-5}
C	4.1132×10^{-5}	---
O	3.7473×10^{-2}	3.3432×10^{-2}
F	2.1474×10^{-4}	---
Na	9.3357×10^{-4}	---
Mg	1.6786×10^{-4}	---
Al	4.2074×10^{-4}	---
Si	2.1125×10^{-3}	---
S	5.0624×10^{-3}	---
K	4.5367×10^{-5}	---
Ca	2.7704×10^{-3}	---
Mn	3.6691×10^{-5}	---
Fe	4.9333×10^{-3}	---
Zn	1.7906×10^{-4}	---
Ba	5.1832×10^{-4}	---

Table 8. Composition of ISSEC Materials and Boral

Element (wt.%)	Material		
	Graphite H-451 Density: 1.74 g/cm^3	TiH_2 Density: 3.76 g/cm^3	Boral Density: 2.53 g/cm^3
H	---	4.04	---
B	---	---	15.7
C	100	---	4.3
Al	---	---	80.0
Ti	---	95.96	---

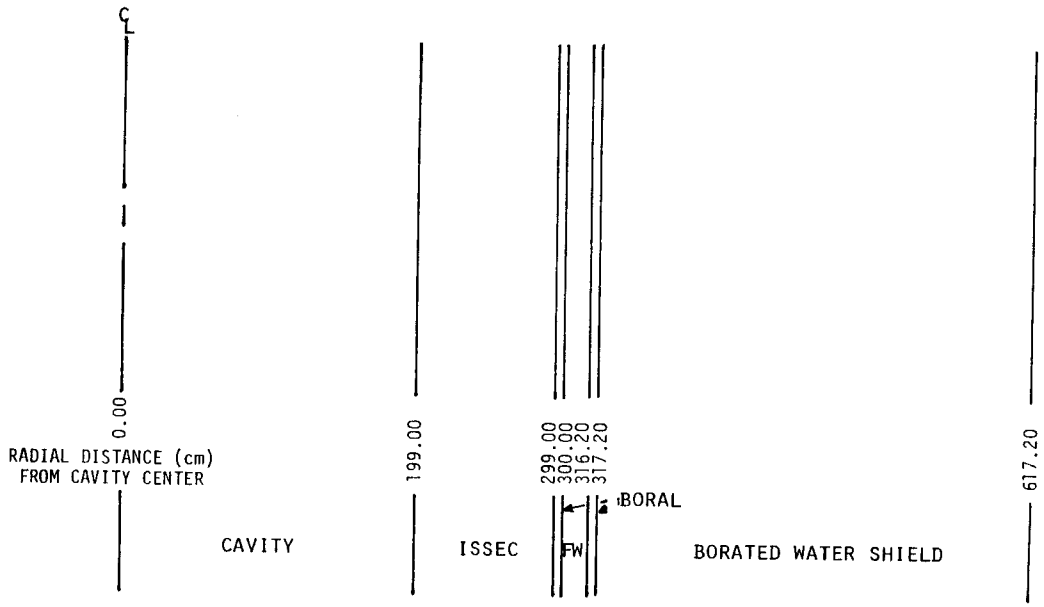

COMPOSITION KEY

ISSEC: GRAPHITE H-451 .4 void fraction
BORAL: Boron (15.7 wt%), Carbon (4.3 wt%), Aluminum (80.0 wt%)
F.W*: Aluminum-6061-T6
SHIELD: Water + 2000 wppm Boron

*See Fig.6 for a note on the Aluminum wall thickness.

Fig. 7. One-dimensional schematic of the Target Development Facility aluminum chamber and shield with graphite ISSEC used for the neutronic and activation calculations.

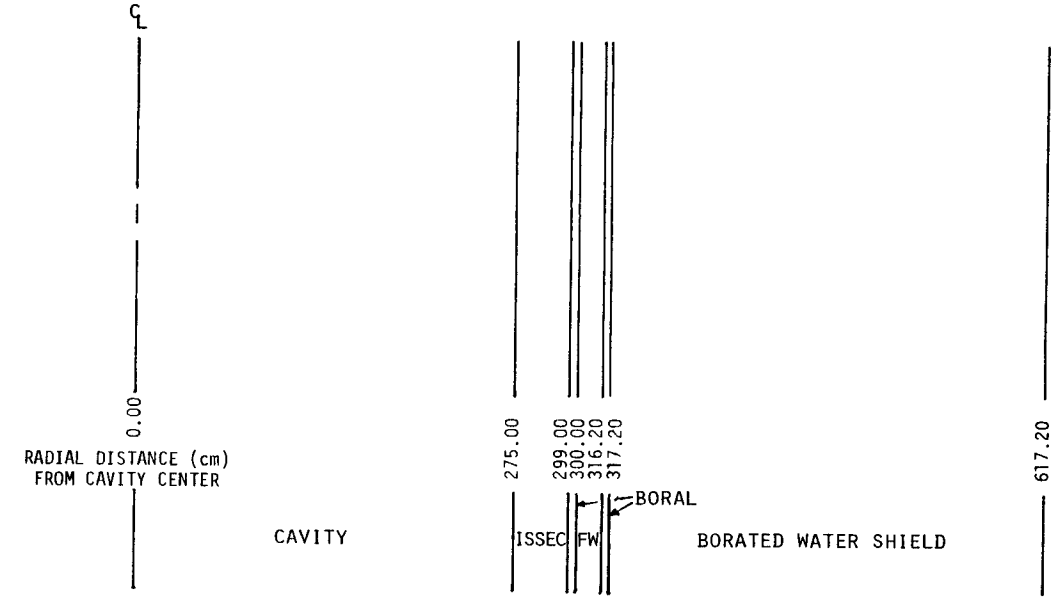

COMPOSITION KEY

ISSEC: TiH_2 (.95*TiH_2 + .05*Aluminum) .1 void fraction
BORAL: Boron (15.7 wt%), Carbon (4.3 wt%), Aluminum (80.0 wt%)
F.W*: Aluminum-6061-T6
SHIELD: Water + 2000 wppm Boron

*See Fig.6 for a note on the Aluminum chamber wall thickness.

Fig. 8. One-dimensional schematic of the Target Development Facility aluminum chamber and shield with TiH_2 ISSEC used for the neutronic and activation calculations.

Table 9. The impurities contained in the graphite which are included in the activation calculations are listed in Table 10.

2.3. Codes and Data Libraries

The transport of neutrons and gamma photons, both in the burning target and throughout the facility, is performed with the one-dimensional discrete ordinates code ANISN.[10] A combined RSIC DLC-41B/VITAMIN-C[11] and DLC-60/MACKLIB-IV[12] 25 neutron-21 gamma group cross-section library containing 48 isotopes with a P_3 Legendre expansion of the scattering cross-sections is used in the calculations. The library is based on ENDF/B-IV.

For the activation calculations the DKR[13] computer code is employed. The DKR code assumes continuous neutron irradiation when computing radioactivity levels and gamma photon sources for selected time periods after shutdown from the scalar flux distribution within the fusion target and the facility. The scalar flux is provided by ANISN. The decay data library used is DCDLIB[14] which contains isotopic radioactive decay and neutron transmutation cross section data from the ENDF/B-IV library, the Table of Isotopes,[15] and selected nuclide data from the ACTL library.[16]

2.4. Calculational Procedure

Two calculational schemes are used to compute dose rates at various positions within the Target Development Facility. The separate computational steps involved are shown in the flowchart diagrams of Fig. 9 for the forward scheme and in Fig. 10 for the adjoint scheme.

The forward scheme is composed of four separate steps to compute decay gamma dose rates. The first step is the determination of the steady state neutron flux throughout the reactor using the one-dimensional transport code ANISN. The input to ANISN consists of neutron sources, neutron cross-

Table 9. Graphite, TiH_2 ISSEC's and Boral Constituent Densities

Element	Graphite ISSEC 0.4 Void Fraction Density [atoms/b-cm]	Graphite ISSEC 0.58 Void Fraction Density [atoms/b-cm]	TiH_2 ISSEC 90% TiH_2 + 10% Al 0.1 Void Fraction	TiH_2 ISSEC 90% TiH_2 + 10% Steel 0.1 Void Fraction	Boral Density [atoms/b-cm]
H	---	---	7.7582×10^{-3}	7.7582×10^{-3}	---
B	1.1633×10^{-7}	8.1428×10^{-8}	---	---	2.2129×10^{-2}
C	5.2351×10^{-2}	3.6646×10^{-2}	---	1.9411×10^{-5}	5.4553×10^{-3}
Na	2.7351×10^{-7}	1.9146×10^{-7}	---	---	---
Mg	2.5864×10^{-8}	1.8105×10^{-8}	3.0101×10^{-5}	---	---
Al	9.3220×10^{-8}	6.5254×10^{-8}	2.6186×10^{-3}	---	4.5181×10^{-2}
Si	4.7016×10^{-7}	3.2911×10^{-7}	1.5634×10^{-5}	3.0154×10^{-5}	---
P	---	---	---	1.3686×10^{-6}	---
S	1.9611×10^{-8}	1.3728×10^{-8}	---	3.8792×10^{-6}	---
Ca	3.4515×10^{-7}	2.4161×10^{-7}	---	---	---
Ti	1.3127×10^{-8}	9.1892×10^{-9}	3.8794×10^{-2}	3.8792×10^{-2}	---
V	1.2343×10^{-8}	8.6404×10^{-9}	---	1.2482×10^{-6}	---
Cr	---	---	4.2223×10^{-6}	8.9676×10^{-5}	---
Mn	---	---	1.9981×10^{-6}	1.9290×10^{-5}	---
Fe	3.3778×10^{-8}	2.3645×10^{-8}	9.1728×10^{-6}	3.6203×10^{-3}	---
Cu	---	---	3.4552×10^{-6}	6.6713×10^{-6}	---
Zn	---	---	2.7987×10^{-6}	---	---
Mo	---	---	---	2.2091×10^{-5}	---
Pb	2.1244×10^{-8}	1.4871×10^{-8}	---	---	---

Table 10. Graphite H-451 Trace Elements (Ref. 9)

Trace Elements	Impurity Content (wppm)
B	2
Na	10
Mg	1
Al	4
Si	21
S	1
Ca	22
Ti	1
V	1
Fe	3
Pb	7

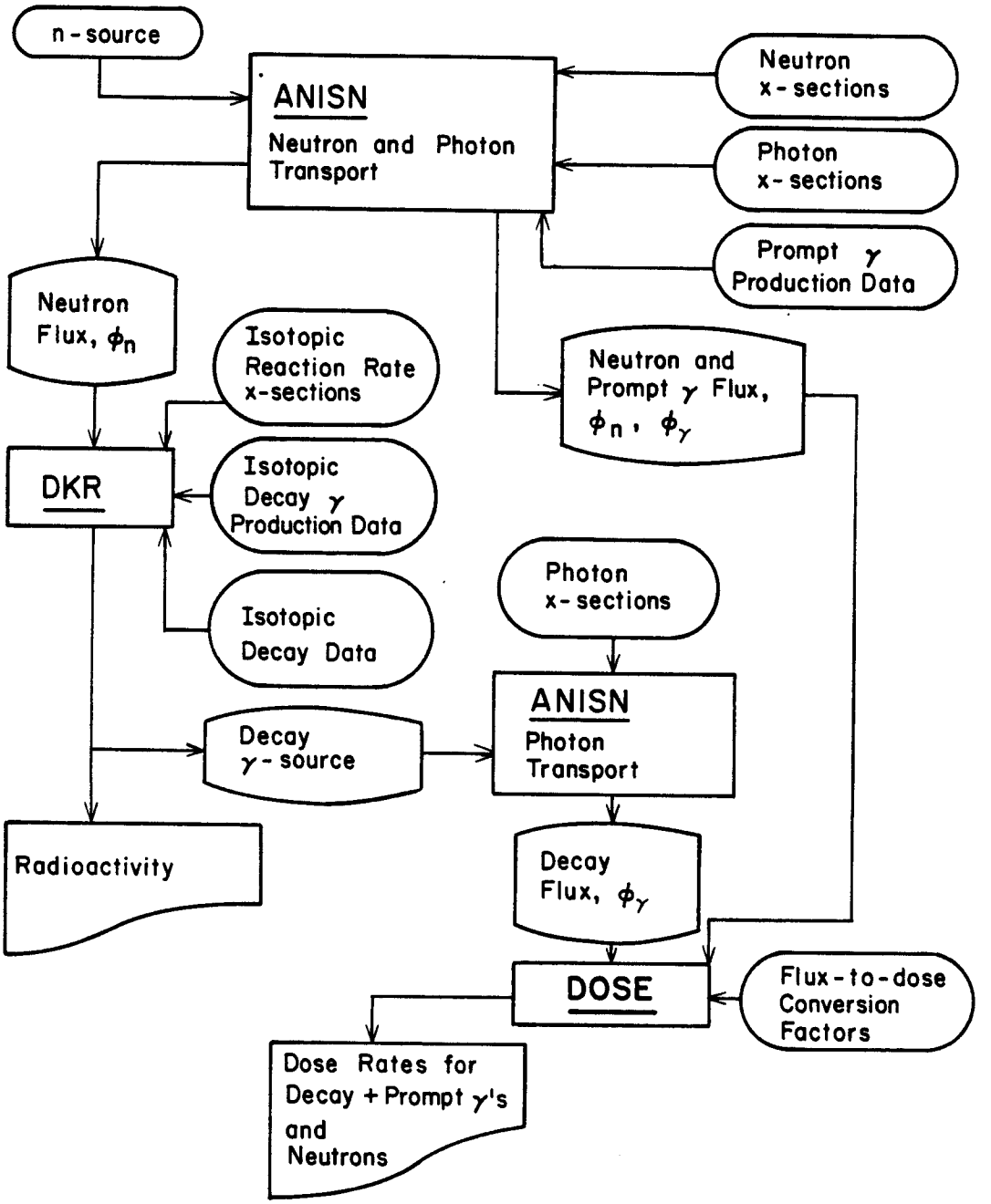

Fig. 9. Flowchart for the calculation of dose rates for the Target Development Facility using the forward scheme.

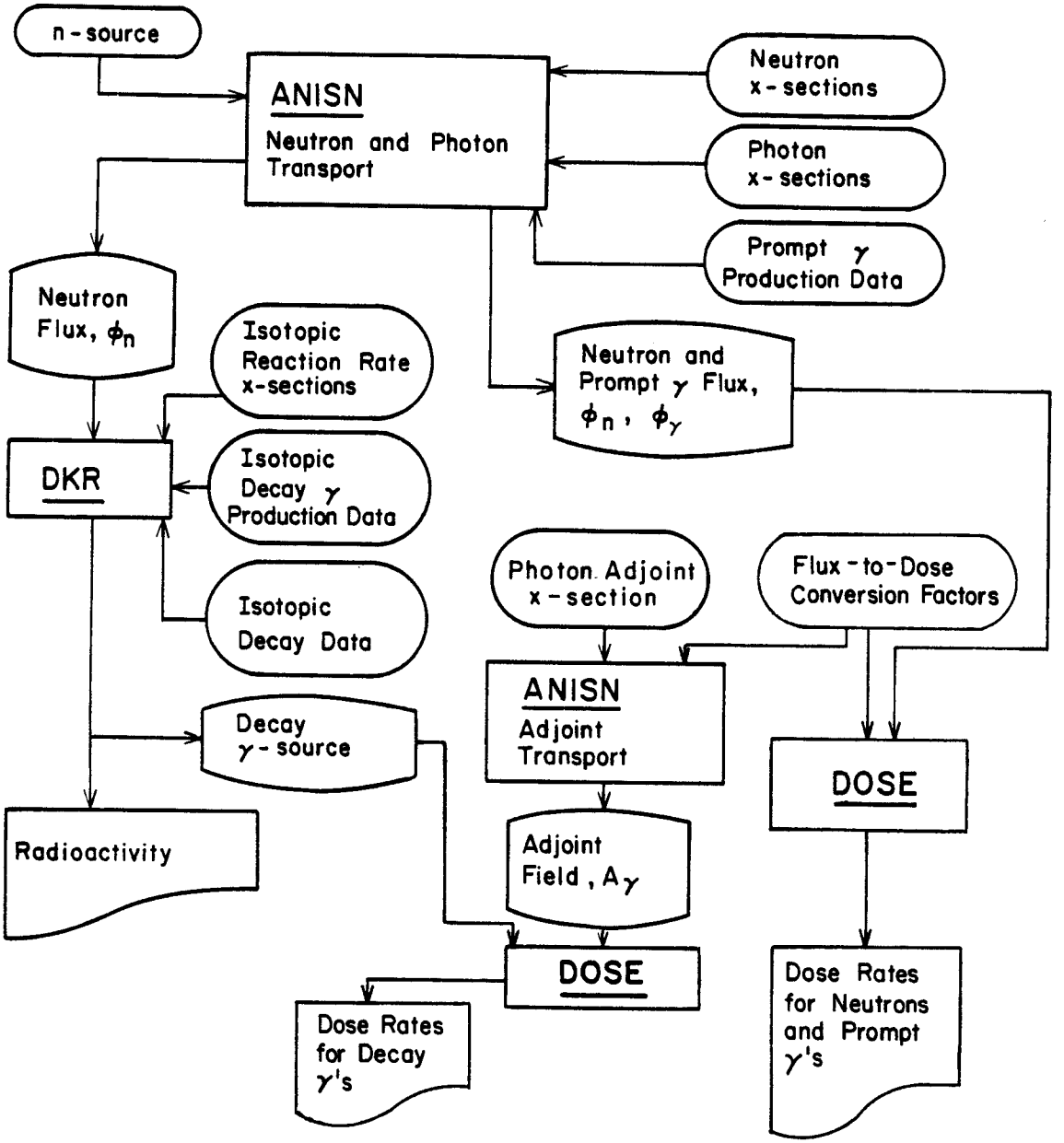

Fig. 10. Flowchart for the calculation of dose rates for the Target Development Facility using the adjoint scheme.

sections, gamma photon cross-sections, and prompt gamma production data. The second step involves the use of the DKR code to compute material activation resulting from neutron transmutation reactions and the computation of the decay gamma source. Determination of the decay gamma source involves multiplying the disintegrations per second of an isotope by its gamma spectrum per decay and summing over all isotopes. The input to DKR consists of the neutron flux, isotopic reaction rate cross-sections, isotopic decay gamma production data, and isotopic decay data (decay constant, mode of decay). The third step is the calculation of the steady state gamma flux throughout the facility using the decay gamma sources and the ANISN transport code. Input for the gamma flux calculations consists of the decay gamma sources computed by the DKR code and the gamma photon cross-sections. The fourth and final step is the multiplication of the gamma flux at a position, r, by the tissue flux-to-dose conversion factors to obtain the dose rate at the position, r. This operation is performed by the auxiliary code DOSE. The neutron and prompt gamma dose rates can be directly computed from the neutron and gamma fluxes throughout the facility by use of DOSE and the tissue flux-to-dose conversion factors (see Fig. 9). A separate DKR and gamma photon transport calculation using ANISN is not required for this calculation.

The adjoint scheme also uses four separate computational steps for the determination of decay gamma dose rates. Steps one and two are identical to those of the forward scheme. Step three is the determination of the adjoint dose field throughout the facility using the ANISN transport code. The input consists of the flux-to-dose conversion factors at the position, r, and the gamma photon adjoint cross-sections. The fourth and final step is the multi-

plication of the adjoint field by the gamma decay sources, which are computed by the DKR code in step two, to obtain the dose rate at the position, r.

The forward scheme is used if it is of interest to obtain the dose rate as a function of position throughout the facility at a specific time after shutdown. The adjoint scheme is employed if the dose rate at a given position, but for various times after shutdown of the facility, is required. Thus, depending on the nature and particular requirements of the problem, the forward or adjoint scheme is chosen. If the dose rate at one position, r', and at one time after shutdown, t', is required, then usually it is more advantageous to use the forward scheme as it provides additional dose rate information at other positions.

3. RESULTS AND DISCUSSION

3.1. Target Radioactivity Analysis

In this section the activation results of the two ion beam targets are analyzed. Since the DT fuel load is 1 mg and the fractional burnup is assumed 30%, the results presented are for approximately 100 MJ of released fusion energy and for one ignited target.

The results of the BeO-W target constituents are shown in Fig. 11. The formation of $^{6}_{2}He$ ($t_{1/2}$ = 0.810 s) and $^{16}_{7}N$ ($t_{1/2}$ = 7.10 s) in the target leads to the very high initial activity of 6.10 x 10^5 curies which decays to the level of 0.3 curies after approximately 2 minutes. The other short lived isotope produced in the target is $^{9}_{3}Li$ ($t_{1/2}$ = 0.178 s) which decays away in less than 1 minute. For times greater than 3 minutes the activity is due to the radioactive isotopes formed by neutron interactions with the W isotopes. Not shown on the figure is the low level long term activity of $^{10}_{4}Be$ ($t_{1/2}$ = 1.62 x 10^6 yrs) and $^{14}_{6}C$ ($t_{1/2}$ = 5734 yrs) which have initial activities of

4.86×10^{-11} curies and 1.29×10^{-15} curies, respectively. For additional details on the production of the radioactive isotopes and the resulting stable isotopes see Table 11. The activity of the unburnt tritium (dashed line) is shown for comparison.

Figure 12 displays the results of the CH_2-Au target constituents. The high initial activity of 1.13×10^3 curies is due to $^{6}_{2}He$. The short lived isotope $^{9}_{3}Li$ is also produced with an initial activity of 18.7 curies. After approximately 3 minutes both isotopes will have decayed away. The remaining radioactive isotopes shown are from neutron interactions on $^{197}_{79}Au$ with the major contributors to the activity after approximately 2 minutes being $^{196}_{79}Au$ and $^{196m}_{79}Au$ (isomeric state of $^{196}_{79}Au$). Both are produced by an (n,2n) reaction with $^{197}_{79}Au$. As with the BeO-W target, the low level long term activity is again due to the $^{10}_{4}Be$ and $^{14}_{6}C$ isotopes which have initial activities of 1.11×10^{-13} curies and 2.07×10^{-14} curies, respectively. The unburnt tritium activity (dashed line) is shown for comparison. Additional information on the production of the radioactive isotopes and resulting stable isotopes can be found in Table 11.

A point to note about the results given above is that for times after shutdown of interest for the facility (1 day, 1 week, 1 month after shutdown), the activity of the targets is solely due to the high-Z tamper material. Thus for the chamber wall and target debris dose rate analysis, only the gamma photons emitted by the decay of the activated tamper materials are considered.

Table 11. Nuclear Decay Chains Considered in the Target Activation Analysis

BeO Pusher-W Tamper Target

isotope $^{9}_{4}Be(n,\alpha)\ ^{6}_{2}He \rightarrow$ decays by β^-, $t_{1/2} = 0.810$ s $\rightarrow\ ^{6}_{3}Li$

$^{9}_{4}Be(n,p)\ ^{9}_{3}Li \rightarrow$ decays by β^-, $t_{1/2} = 0.178$ s $\rightarrow\ ^{9}_{4}Be$

$^{9}_{4}Be(n,\gamma)\ ^{10}_{4}Be \rightarrow$ decays by β^-, $t_{1/2} = 1.62 \times 10^{6}$ yrs $\rightarrow\ ^{10}_{5}B$

isotope $^{16}_{8}O(n,p)\ ^{16}_{7}N \rightarrow$ decays by β^-, $t_{1/2} = 7.10$ s $\rightarrow\ ^{16}_{8}O$

$^{16}_{8}O(n,\alpha)\ ^{13}_{6}C \rightarrow\ ^{13}_{6}C(n,\gamma)\ ^{14}_{6}C \rightarrow$ decays by β^-, $t_{1/2} = 5734$ yrs $\rightarrow\ ^{14}_{7}N$

isotope $^{182}_{74}W(n,p)\ ^{182}_{73}Ta \rightarrow$ decays by β^-, $t_{1/2} = 115$ days $\rightarrow\ ^{182}_{74}W$

$^{182}_{74}W(n,2n)\ ^{181}_{74}W \rightarrow$ decays by EC, $t_{1/2} = 121$ days $\rightarrow\ ^{181}_{73}Ta$

$^{182}_{74}W(n,\gamma)\ ^{183}_{74}W \rightarrow\ ^{183}_{74}W(n,n')p\ ^{182}_{73}Ta \rightarrow$ decays by β^-, $t_{1/2} = 115$ days $\rightarrow\ ^{182}_{74}W$

$^{182}_{74}W(n,\gamma)\ ^{183}_{74}W \rightarrow\ ^{183}_{74}W(n,p)\ ^{183}_{73}Ta \rightarrow$ decays by β^-, $t_{1/2} = 5.0$ days $\rightarrow\ ^{183}_{74}W$

isotope $^{183}_{74}W(n,d)\ ^{182}_{74}W(n,n')p\ ^{182}_{73}Ta \rightarrow$ decays by β^-, $t_{1/2} = 115$ days $\rightarrow\ ^{182}_{74}W$

$^{183}_{74}W(n,p)\ ^{183}_{73}Ta \rightarrow$ decays by β^-, $t_{1/2} = 5.0$ days $\rightarrow\ ^{183}_{74}W$

$^{183}_{74}W(n,2n)\ ^{182}_{74}W \rightarrow\ ^{182}_{74}W(n,p)\ ^{182}_{73}Ta \rightarrow$ decays by β^-, $t_{1/2} = 115$ days $\rightarrow\ ^{182}_{74}W$

$^{183}_{74}W(n,2n)\ ^{182}_{74}W \rightarrow\ ^{182}_{74}W(n,2n)\ ^{181}_{74}W \rightarrow$ decays by EC, $t_{1/2} = 121$ days $\rightarrow\ ^{181}_{73}Ta$

$^{183}_{74}W(n,\gamma)\ ^{184}_{74}W \rightarrow\ ^{184}_{74}W(n,\alpha)\ ^{181}_{72}Hf \rightarrow$ decays by β^-, $t_{1/2} = 42.7$ days $\rightarrow\ ^{181}_{73}Ta$

$^{183}_{74}W(n,\gamma)\ ^{184}_{74}W \rightarrow\ ^{184}_{74}W(n,n')p\ ^{183}_{73}Ta \rightarrow$ decays by β^-, $t_{1/2} = 5.0$ days $\rightarrow\ ^{183}_{74}W$

$^{183}_{74}W(n,\gamma)\ ^{184}_{74}W \rightarrow\ ^{184}_{74}W(n,p)\ ^{184}_{73}Ta \rightarrow$ decays by β^-, $t_{1/2}$ = 8.7 hrs $\rightarrow\ ^{184}_{74}W$

$^{183}_{74}W(n,\gamma)\ ^{184}_{74}W \rightarrow\ ^{184}_{74}W(n,\gamma)\ ^{185}_{74}W \rightarrow$ decays by β^-, $t_{1/2}$ = 75.1 days $\rightarrow\ ^{185}_{75}Re$

isotope $^{184}_{74}W(n,\alpha)\ ^{181}_{72}Hf \rightarrow$ decays by β^-, $t_{1/2}$ = 42.7 days $\rightarrow\ ^{181}_{73}Ta$

$^{184}_{74}W(n,d)\ ^{183}_{(n,n')p}\ ^{183}_{73}Ta \rightarrow$ decays by β^-, $t_{1/2}$ = 5.0 days $\rightarrow\ ^{183}_{74}W$

$^{184}_{74}W(n,p)\ ^{184}_{73}Ta \rightarrow$ decays by β^-, $t_{1/2}$ = 8.7 hrs $\rightarrow\ ^{184}_{74}W$

$^{184}_{74}W(n,\gamma)\ ^{185}_{74}W \rightarrow$ decays by β^-, $t_{1/2}$ = 75.1 days $\rightarrow\ ^{185}_{75}Re$

$^{184}_{74}W(n,2n)\ ^{183}_{74}W \rightarrow\ ^{183}_{74}W(n,d)\ ^{183}_{(n,n')p}\ ^{182}_{73}Ta \rightarrow$ decays by β^-, $t_{1/2}$ = 115 days $\rightarrow\ ^{182}_{74}W$

$^{184}_{74}W(n,2n)\ ^{183}_{74}W \rightarrow\ ^{183}_{74}W(n,p)\ ^{183}_{73}Ta \rightarrow$ decays by β^-, $t_{1/2}$ = 5.0 days $\rightarrow\ ^{183}_{74}W$

$^{184}_{74}W(n,2n)\ ^{183}_{74}W \rightarrow\ ^{183}_{74}W(n,2n)\ ^{182}_{74}W \rightarrow\ ^{182}_{74}W(n,p)\ ^{182}_{73}Ta \rightarrow$ decays by β^-,

$t_{1/2}$ = 115 days $\rightarrow\ ^{182}_{74}W$

$^{184}_{74}W(n,2n)\ ^{183}_{74}W \rightarrow\ ^{183}_{74}W(n,2n)\ ^{182}_{74}W \rightarrow\ ^{182}_{74}W(n,2n)\ ^{181}_{74}W \rightarrow$ decays by EC,

$t_{1/2}$ = 121 days $\rightarrow\ ^{181}_{73}Ta$

isotope $^{186}_{74}W(n,p)\ ^{186}_{73}Ta \rightarrow$ decays by β^-, $t_{1/2}$ = 10.6 min $\rightarrow\ ^{186}_{74}W$

$^{186}_{74}W(n,2n)\ ^{185}_{74}W \rightarrow$ decays by β^-, $t_{1/2}$ = 75.1 days $\rightarrow\ ^{185}_{75}Re$

$^{186}_{74}W(n,\gamma)\ ^{187}_{74}W \rightarrow$ decays by β^-, $t_{1/2}$ = 23.9 hrs $\rightarrow\ ^{187}_{75}Re$

$^{186}_{74}W(n,\alpha)\ ^{183}_{72}Hf \rightarrow$ decays by β^-, $t_{1/2}$ = 1.06 hrs $\rightarrow\ ^{183}_{73}Ta \rightarrow$ decays by β^-,

$t_{1/2}$ = 5.0 days $\rightarrow\ ^{183}_{74}W$

isotope $^{186}_{74}W(n,d)\,(n,n')p\ ^{185}_{73}Ta \rightarrow$ decays by β^-, $t_{1/2}$ = 49.5 min $\rightarrow\ ^{185}_{74}W \rightarrow$ decays by β^-, $t_{1/2}$ = 75.1 days $\rightarrow\ ^{185}_{75}Re$

CH_2 Pusher-Au Tamper Target

isotope $^{12}_{6}C(n,\alpha)\ ^{9}_{4}Be \rightarrow\ ^{9}_{4}Be(n,\alpha)\ ^{6}_{2}He \rightarrow$ decays by β^-, $t_{1/2}$ = 0.810s $\rightarrow\ ^{6}_{3}Li$

$^{12}_{6}C(n,\alpha)\ ^{9}_{4}Be \rightarrow\ ^{9}_{4}Be(n,p)\ ^{9}_{3}Li \rightarrow$ decays by β^-, $t_{1/2}$ = 0.178 s $\rightarrow\ ^{9}_{4}Be$

$^{12}_{6}C(n,\alpha)\ ^{9}_{4}Be \rightarrow\ ^{9}_{4}Be(n,\gamma)\ ^{10}_{4}Be \rightarrow$ decays by β^-, $t_{1/2}$ = 1.62 x 10^6 yrs $\rightarrow\ ^{10}_{5}B$

isotope $^{13}_{6}C(n,\gamma)\ ^{14}_{6}C \rightarrow$ decays by β^-, $t_{1/2}$ = 5734 yrs $\rightarrow\ ^{14}_{7}N$

isotope $^{197}_{79}Au(n,\alpha)\ ^{194}_{77}Ir \rightarrow$ decays by β^-, $t_{1/2}$ = 19.15 hrs $\rightarrow\ ^{194}_{78}Pt$

$^{197}_{79}Au(n,2n)\ ^{196}_{79}Au \rightarrow$ decays by EC, $t_{1/2}$ = 6.17 days $\rightarrow\ ^{196}_{78}Pt$

$^{197}_{79}Au(n,\gamma)\ ^{198}_{79}Au \rightarrow$ decays by β^-, $t_{1/2}$ = 2.67 days $\rightarrow\ ^{198}_{80}Hg$

$^{197}_{79}Au(n,2n)\ ^{196}_{79}Au^{*} \rightarrow$ decays by γ, $t_{1/2}$ = 9.7 hrs $\rightarrow\ ^{196}_{79}Au \rightarrow$ decays by EC, $t_{1/2}$ = 6.17 days $\rightarrow\ ^{196}_{78}Pt$

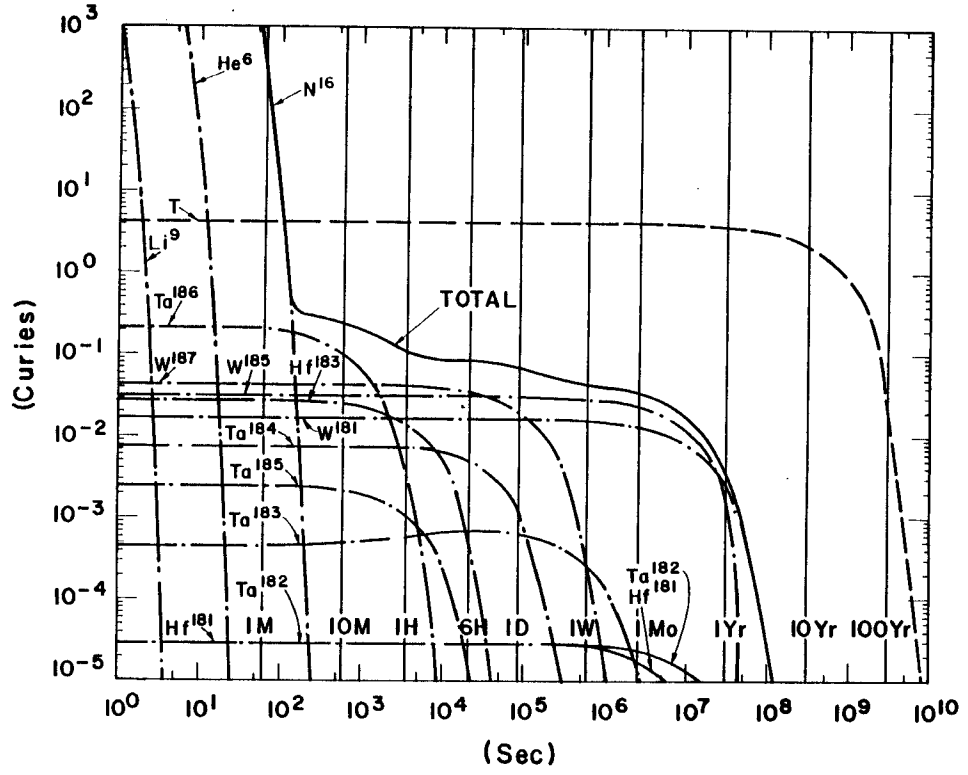

Fig. 11. Isotopic activation versus time for the BeO-W target.

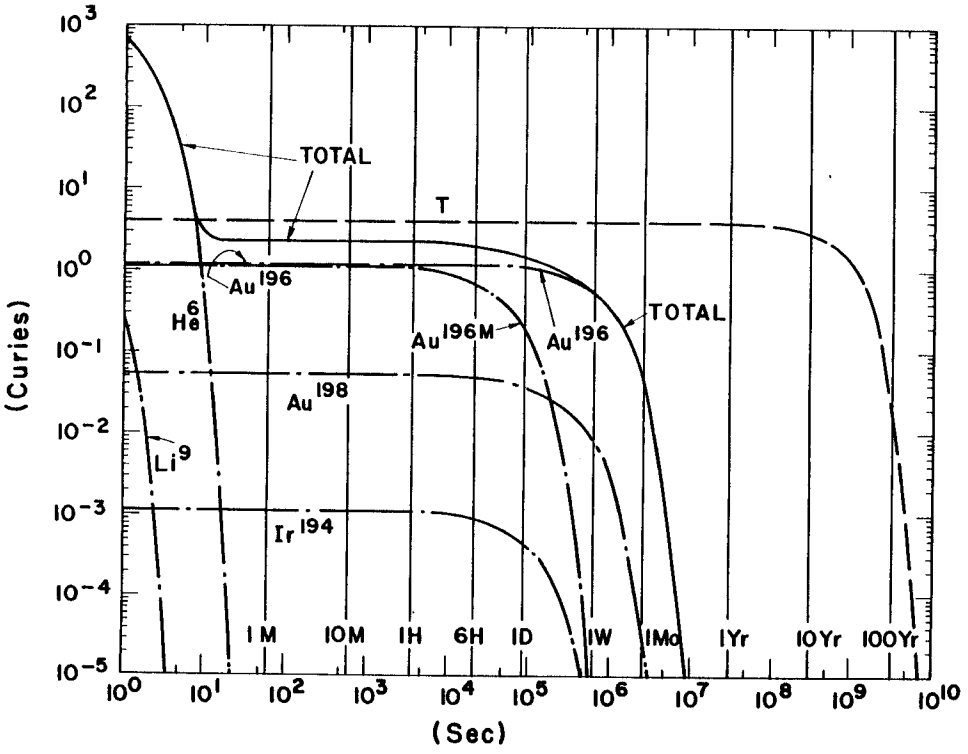

Fig. 12. Isotopic activation versus time for the CH_2-Au target.

3.2 Chamber Wall Analysis

All of the chamber wall and target debris dose rates presented in this section are normalized to a target yield of 200 MJ and 3120 shots per year. The biological dose rates of the accumulated target debris (BeO-W and CH_2-Au targets), and the steel and aluminum chamber walls have been compared at shutdown and 1 day, 1 week, 1 month and 1 year after shutdown for the borated water pool design. Table 12 presents the results for the biological dose rates at the inner surface of the first wall upon which the target debris has accumulated. Histograms comparing the dose contribution from the steel wall and alternatively, the Au debris and W debris, as a function of time after shutdown are given in Fig. 13. A similar comparison for the aluminum wall is given in Fig. 14 and a comparison of the steel and aluminum walls is plotted on Fig. 15. As mentioned in Section 3.1, only the gamma sources of the tamper materials are considered in the calculations of the target debris dose rates. Several points to note are:

1. A comparison between the dose rates of the accumulated target debris shows that the dose rate of the Au debris is approximately two orders of magnitude higher than that of the W debris through 1 month after shutdown. This changes as the activity of the Au debris decreases rapidly after approximately 3 months (see Fig. 12). At 1 year after shutdown the dose rate of the W debris is 2.5 mrem/hr whereas that of the Au debris has become negligibly small.
2. The dose rate of the aluminum chamber wall is larger than that of the steel up to approximately 1 day after shutdown. After a period of 1 week the dose rate of the steel exceeds that of the aluminum.

Table 12. Dose Rate (mrem/hr) at Inner Surface of First Wall

	T = 0	T = 1 day	T = 1 wk	T = 1 mo	T = 1 yr
Aluminum First Wall	6.44×10^{6}	1.12×10^{6}	4.26×10^{3}	2.48×10^{3}	1.02×10^{3}
Au (with Al F.W.)	3.05×10^{4}	2.95×10^{4}	1.51×10^{4}	1.08×10^{3}	5.0×10^{-14}
W (with Al F.W.)	6.25×10^{2}	1.88×10^{2}	4.07×10^{1}	2.42×10^{1}	2.49
Steel First Wall	8.54×10^{5}	6.39×10^{4}	5.96×10^{4}	5.22×10^{4}	1.98×10^{4}
Au (with Steel F.W.)	2.72×10^{4}	2.63×10^{4}	1.35×10^{4}	9.57×10^{2}	4.4×10^{-14}
W (with Steel F.W.)	5.84×10^{2}	1.77×10^{2}	3.80×10^{1}	2.33×10^{1}	2.43
Aluminum + Au	6.47×10^{6}	1.15×10^{6}	1.94×10^{4}	3.56×10^{3}	1.02×10^{3}
Aluminum + W	6.44×10^{6}	1.12×10^{6}	4.30×10^{3}	2.50×10^{3}	1.02×10^{3}
Steel + Au	8.81×10^{5}	9.02×10^{4}	7.31×10^{4}	5.32×10^{4}	1.98×10^{4}
Steel + W	8.55×10^{5}	6.41×10^{4}	5.96×10^{4}	5.22×10^{4}	1.98×10^{4}

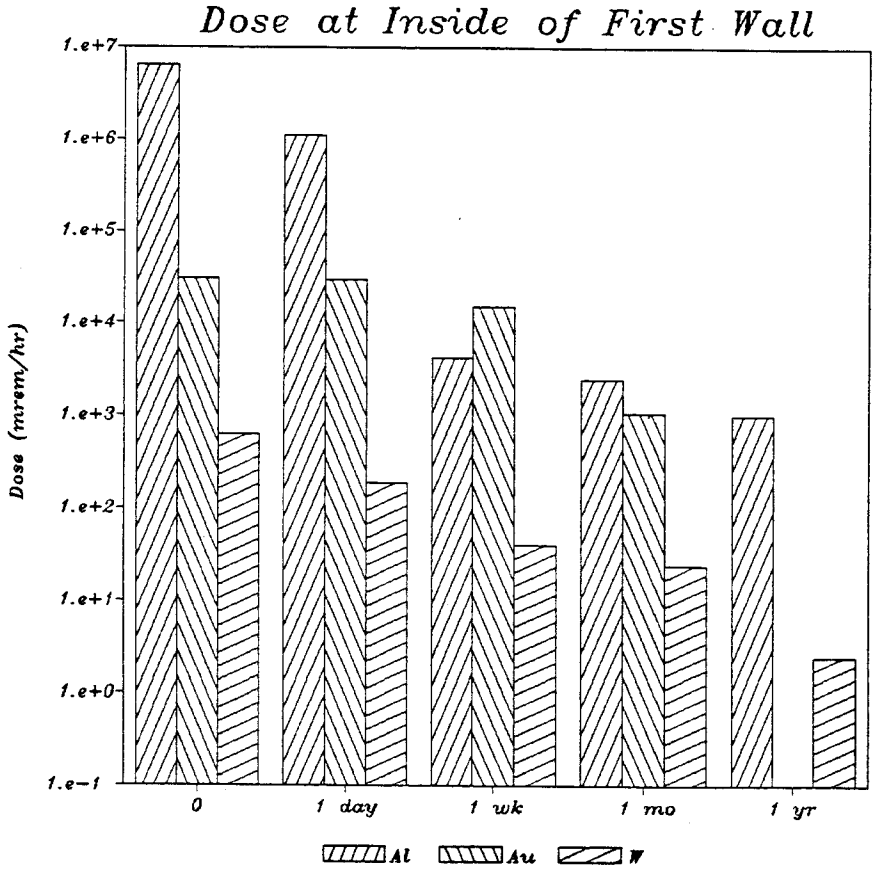

Fig. 13. A comparison of the aluminum wall structure, Au and W target debris dose rates at the inner surface of the chamber.

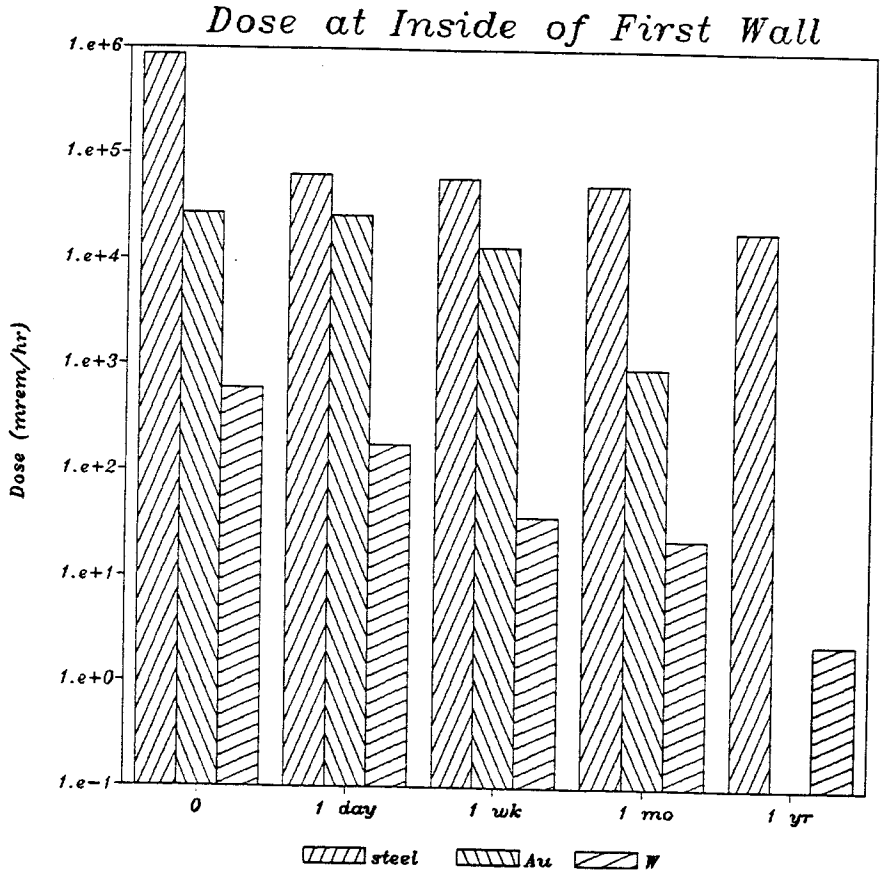

Fig. 14. A comparison of the steel wall structure, Au and W target debris dose rates at the inner surface of the chamber.

3. The dose rate of both chamber materials is seen to be considerably larger than that due to the W debris, whereas the dose rate of the Au debris is comparable to the steel at 1 day and 1 week after shutdown and is larger than that of the aluminum at 1 week after shutdown.

Thus one can conclude that at the inner surface of the chamber, depending on the target material composition, the dose rate due to the accumulated target debris can become comparable to that of the chamber itself. Since a liner on the inside of the chamber wall is being considered for protection of the wall from thermal effects of the target explosion, the condensable target debris collected on the liner could be periodically removed, thereby reducing the dose rate component due to the target debris at the inner surface of the chamber wall. Elimination of the Au debris would reduce the combined aluminum wall plus Au debris dose rate to approximately 22% of its present value and the combined steel wall plus Au debris dose rate to approximately 81.5% of its present value at 1 week after shutdown. Even with this reduction, the dose rate within the chamber remains too high for hands on maintenance.

It may be possible to perform underwater maintenance with the water shield in place. The biological dose rate a diver would receive at the outer surface of the target chamber is presented in Table 13. Histograms of various comparisons are displayed in Figs. 16, 17 and 18. Here, as with the dose rates at the inner surface, the target debris dose rate of the Au exceeds that of the W until approximately 3 months after shutdown. Also, the dose rate of the aluminum chamber exceeds that of the steel chamber, but after a 1 week shutdown period, the steel chamber dose rate is larger. One notices now, however, that the target debris dose rate at the outer surface is considerably lower than that of the chamber materials. This is because the gamma photons

Table 13. Dose Rate (mrem/hr) at Outer Surface of First Wall

	T = 0	T = 1 day	T = 1 wk	T = 1 mo	T = 1 yr
Aluminum First Wall	2.75×10^{6}	3.61×10^{5}	1.29×10^{3}	7.18×10^{2}	2.84×10^{2}
Au (with Al F.W.)	4.84×10^{2}	4.66×10^{2}	2.36×10^{2}	1.66×10^{1}	7.7×10^{-16}
W (with Al F.W.)	1.69×10^{1}	5.32	1.27	9.17×10^{-1}	1.04×10^{-1}
Steel First Wall	6.69×10^{5}	3.82×10^{4}	3.54×10^{4}	2.94×10^{4}	8.90×10^{3}
Au (with Steel F.W.)	7.65×10^{2}	7.33×10^{2}	3.68×10^{2}	2.58×10^{1}	1.2×10^{-15}
W (with Steel F.W.)	3.21×10^{1}	1.02×10^{1}	2.38	1.78	2.02×10^{-1}
Aluminum + Au	2.75×10^{6}	3.61×10^{5}	1.53×10^{3}	7.35×10^{2}	2.84×10^{2}
Aluminum + W	2.75×10^{6}	3.61×10^{5}	1.29×10^{3}	7.19×10^{2}	2.84×10^{2}
Steel + Au	6.70×10^{5}	3.89×10^{4}	3.58×10^{4}	2.94×10^{4}	8.90×10^{3}
Steel + W	6.69×10^{5}	3.82×10^{4}	3.54×10^{4}	2.94×10^{4}	8.90×10^{3}

Table 14. Dose (mrem/hr) at 27.5 cm from Outer Surface of First Wall

	T = 0	T = 1 day	T = 1 wk	T = 1 mo	T = 1 yr
Aluminum First Wall	5.75×10^{5}	7.66×10^{4}	2.14×10^{2}	1.01×10^{2}	4.06×10^{1}
Au (with Al F.W.)	5.67×10^{1}	5.42×10^{1}	2.71×10^{1}	1.90	8.79×10^{-17}
W (with Al F.W.)	2.76	8.94×10^{-1}	2.35×10^{-1}	1.79×10^{-1}	2.09×10^{-2}
Steel First Wall	2.32×10^{5}	5.18×10^{3}	4.80×10^{3}	3.99×10^{3}	1.20×10^{3}
Au (with Steel F.W.)	1.02×10^{2}	9.71×10^{1}	4.82×10^{1}	3.36	1.56×10^{-16}
W (with Steel F.W.)	5.55	1.80	4.55×10^{-1}	3.49×10^{-1}	4.06×10^{-2}
Aluminum + Au	5.75×10^{5}	7.67×10^{4}	2.41×10^{2}	1.03×10^{2}	4.06×10^{1}
Aluminum + W	5.75×10^{5}	7.66×10^{4}	2.14×10^{2}	1.01×10^{2}	4.06×10^{1}
Steel + Au	2.32×10^{5}	5.28×10^{3}	4.85×10^{3}	3.99×10^{3}	1.20×10^{3}
Steel + W	2.32×10^{5}	5.18×10^{3}	4.80×10^{3}	3.99×10^{3}	1.20×10^{3}

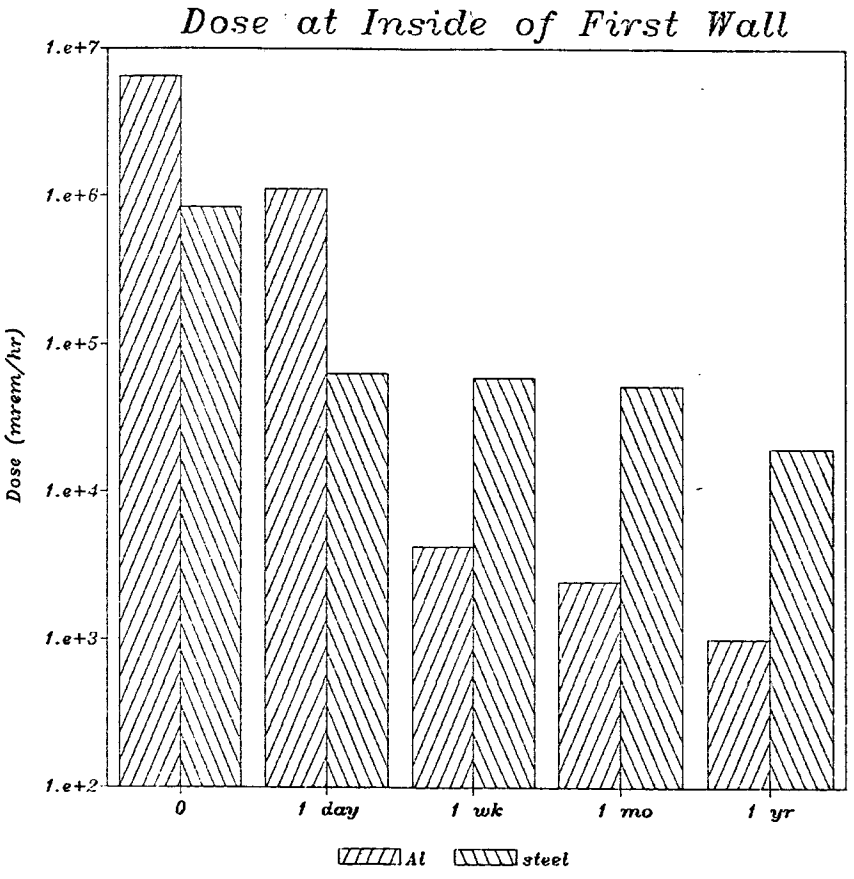

Fig. 15. A comparison of the aluminum and steel wall structure dose rates at the inner surface of the chamber.

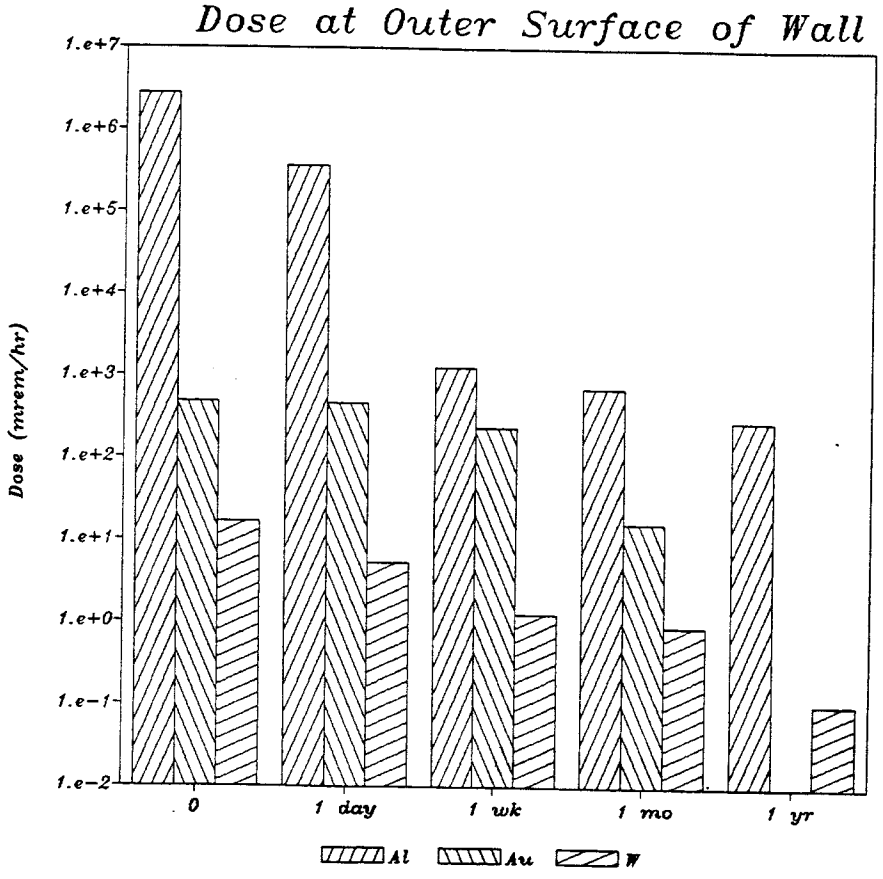

Fig. 16. A comparison of the aluminum wall structure, Au and W target debris dose rates at the outer surface of the chamber.

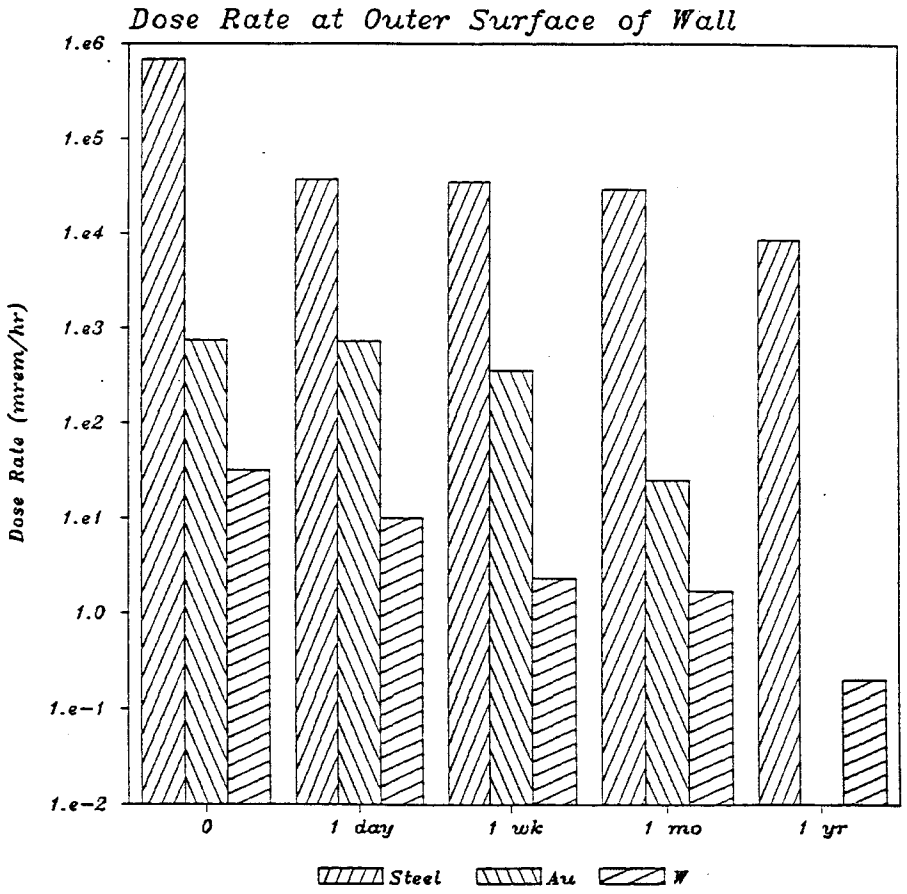

Fig. 17. A comparison of the steel wall structure, Au and W target debris dose rates at the outer surface of the chamber.

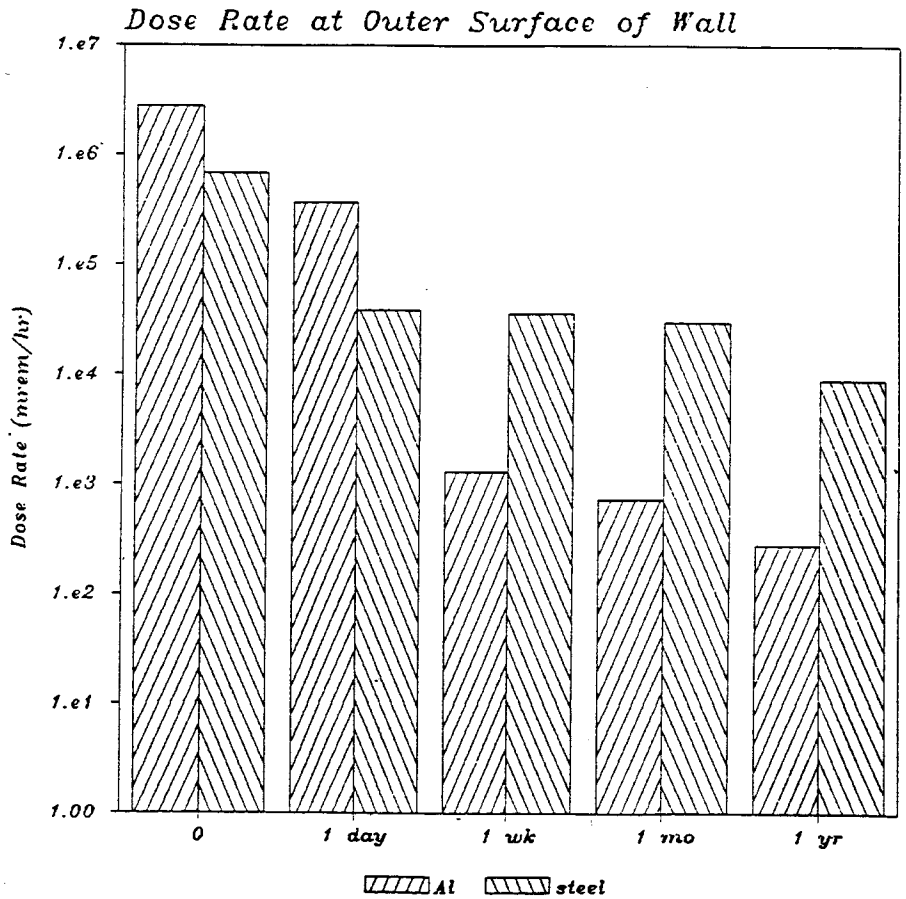

Fig. 18. A comparison of the aluminum and steel wall structure dose rates at the outer surface of the chamber.

emitted by the accumulated target debris can be considered as emanating from a surface source and hence are attenuated as they pass through the chamber wall, decreasing the target debris component to the outer surface dose rate. Thus, the dose rates exterior to the chamber wall can essentially be considered to be that of the chamber wall materials. This is again seen in Table 14 which presents the dose rates at 27.5 cm from the outer surface of the chamber wall with borated water in between.

The dose rate a person would receive standing at the edge of the borated water shield at shutdown is 10.2 mrem/hr for the aluminum chamber and 20.5 mrem/hr for the steel chamber. One day after shutdown these values are reduced to 0.25 mrem/hr for the aluminum and 1.7×10^{-4} mrem/hr for the steel. The values at shutdown reflect the activity of the borated water shield, in particular the $^{16}_{7}N$ isotope which has a 7.1 s half-life. After about 5 to 6 minutes after shutdown the activity of $^{16}_{7}N$ is negligible, therefore the dose rates will be reduced to approximately the values given at 1 day. Further remarks regarding the production of $^{16}_{7}N$ within the borated water shield are given in Section 3.5.

From Fig. 19 one notices that even though the dose rates of the aluminum and steel chamber walls differ approximately by 1 order of magnitude at the outer surface at 1 day after shutdown, the difference increases to approximately 3 orders of magnitude at the shield's edge. This is a direct result of the higher energy gamma photons released by the activated aluminum material. This can be seen in Table 15 which presents the approximate gamma photon source strength densities of each energy interval at 1 day and 1 week after shutdown for the aluminum and steel chamber materials. The high energy gamma photons released in aluminum are due to the $^{24}_{11}Na$ radioactive isotope (see

Table 15. Approximate Gamma Photon Source Density of Chamber Wall Material

Energy Interval (MeV)	At 1 Day After Shutdown: Steel Wall (γ/cm^3-s)	At 1 Day After Shutdown: Aluminum Wall (γ/cm^3-s)
3.0-2.5	---	$\sim 10^7$
2.5-2.0	$\sim 10^4$	$\sim 10^2$
2.0-1.5	$\sim 10^4$	$\sim 10^3$
1.5-1.0	$\sim 10^6$	$\sim 10^6$
1.0-0.4	$\sim 10^6$	$\sim 10^5$
0.4-0.2	$\sim 10^5$	$\sim 10^4$
0.2-0.1	$\sim 10^5$	$\sim 10^3$
0.1-0.01	$\sim 10^4$	$\sim 10^{-1}$

Energy Interval (MeV)	At 1 Week After Shutdown: Steel Wall (γ/cm^3-s)	At 1 Week After Shutdown: Aluminum Wall (γ/cm^3-s)
3.0-2.5	---	$\sim 10^4$
2.5-2.0	---	---
2.0-1.5	$\sim 10^4$	$\sim 10^2$
1.5-1.0	$\sim 10^6$	$\sim 10^4$
1.0-0.4	$\sim 10^6$	$\sim 10^4$
0.4-0.2	$\sim 10^5$	$\sim 10^4$
0.2-0.1	$\sim 10^5$	$\sim 10^3$
0.1-0.01	$\sim 10^3$	$\sim 10^{-1}$

Table 18). This gamma ray has a smaller attenuation coefficient in water than does that of gammas produced by steel. Hence, the higher energy gammas of the aluminum are not attenuated as strongly as the lower energy gammas from the steel, resulting in diverging dose rate curves. This can once again be seen in Fig. 20 which shows the dose rates in the borated water shield as a function of position from the chamber wall outer surface at 1 week after shutdown. Here the dose rate at the outer surface of the steel chamber is approximately 1 order of magnitude larger than that of the aluminum. At the shield's edge the dose rates are comparable with steel having a dose rate of 1.2×10^{-4} mrem/hr and aluminum having a dose rate of 3.2×10^{-4} mrem/hr.

To consider the dose rates in the bay area above the water pool, one notices from Figs. 19 and 20 that the 3 meters of borated water provides more than an adequate amount of shielding. This can be seen by the occupational dose rate limit of 2.4 mrem/hr indicated in the figures. For the steel chamber, the thickness of the borated water shield could be reduced by half its thickness, to 1.50 meters, and for the aluminum chamber, the shield thickness could be reduced to 2.60 meters at 1 day after shutdown.

The contribution of the neutron albedo from the borated water shield to the dose rates in the wall was investigated with the results presented in Table 16. The case labeled "with borated water shield" represents the dose rate calculation for the present preliminary design. The case labeled "without borated water shield" has the shield replaced by vacuum thereby simulating an idealized zero neutron albedo boundary condition (i.e., no neutron return current from the shield) and thus represents the best possible situation. Hence, the difference between the computed dose rates is attributed to the neutron albedo. From Table 16 one notices that the neutron albedo contri-

Table 16. Dose in mrem/hr at Aluminum First Wall Outer Surface

Time	With Borated Water Shield	Without Borated Water Shield	Neutron Albedo Contribution
0	2.75×10^{6}	1.19×10^{6}	56.73%
1 day	3.61×10^{5}	3.26×10^{5}	9.70%
1 week	1.29×10^{3}	1.04×10^{3}	19.38%
1 month	7.18×10^{2}	5.59×10^{2}	22.14%
1 year	2.84×10^{2}	2.39×10^{2}	15.85%

Dose in mrem/hr at Steel First Wall Outer Surface

Time	With Borated Water Shield	Without Borated Water Shield	Neutron Albedo Contribution
0	6.69×10^{5}	2.74×10^{5}	59.04%
1 day	3.82×10^{4}	1.75×10^{4}	54.19%
1 week	3.54×10^{4}	1.65×10^{4}	53.39%
1 month	2.94×10^{4}	1.55×10^{4}	47.28%
1 year	8.90×10^{4}	7.23×10^{3}	18.76%

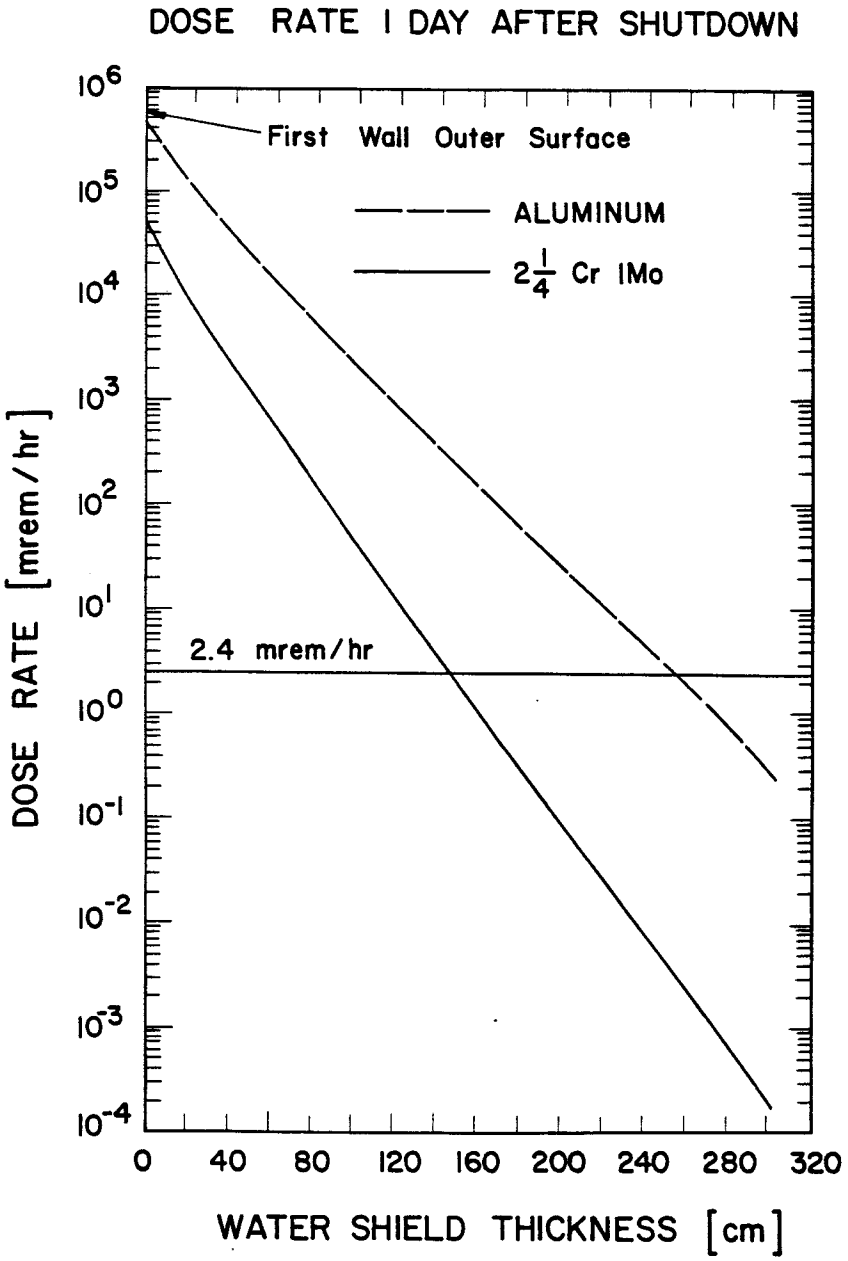

Fig. 19. Dose rate vs. distance from outer surface of the aluminum and steel chamber walls 1 day after shutdown.

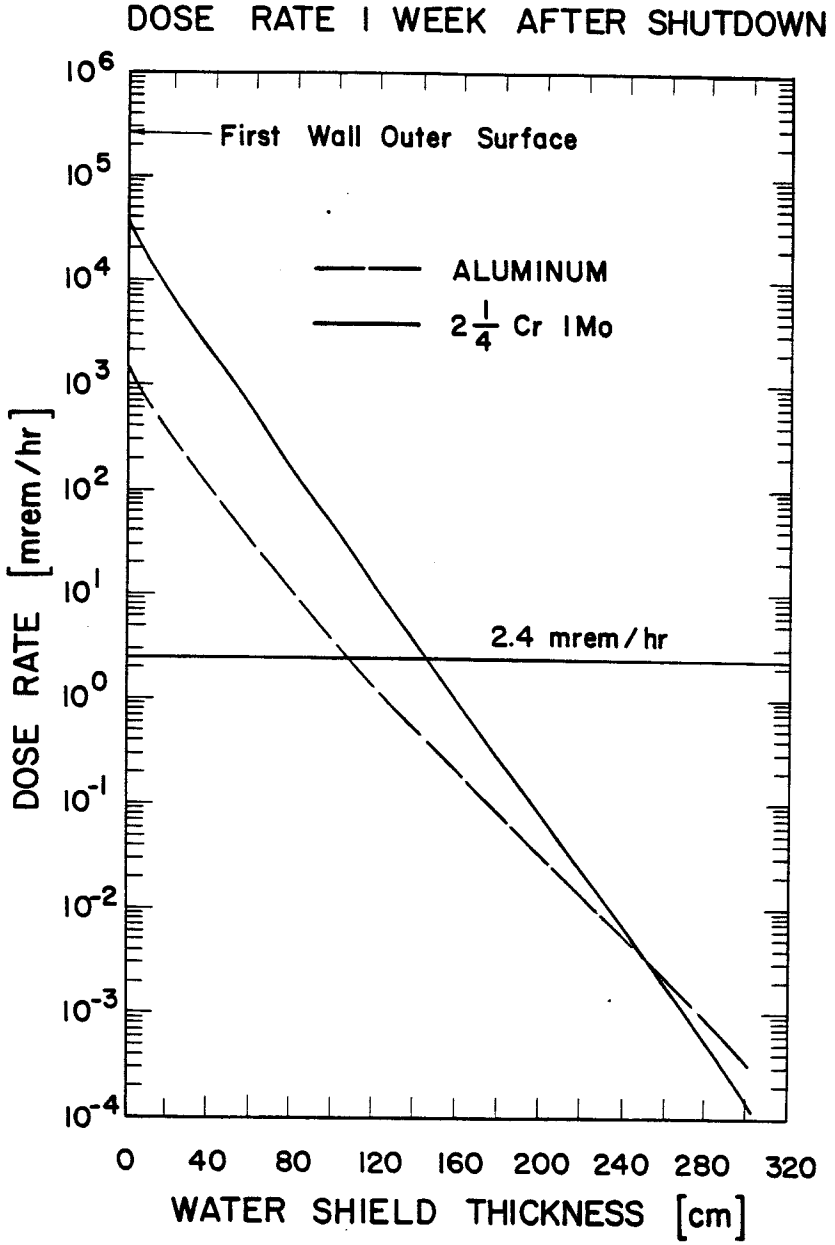

Fig. 20. Dose rate vs. distance from outer surface of the aluminum and steel chamber walls 1 week after shutdown.

bution changes with the time after shutdown. This is because the individual isotopes contributing to the decay gamma source all decay with different decay constants. Hence, the chamber wall decay gamma sources have a time dependence similar to the target activation curves in Figs. 11 and 12. At 1 day and 1 week after shutdown, the neutron albedo component contributes more than 50 percent of the steel dose rate compared to only 9.7 and 19.4 percent for the aluminum chamber wall. Thus, the total dose can be reduced by roughly a factor of 2 for the steel chamber and 1.1 and 1.25 for the aluminum chamber by increasing the weight percent boron in the borated water shield or by placement of a boral shield on the outer surface of the wall. This reduction does not offer any qualitative difference in the dose rate problem at the wall surface; it still remains too high for hands on maintenance.

An examination of the nuclide decay chains given by the DKR code shows that the remaining dose rate component is mainly the result of neutron transmutation reactions above neutron threshold values in the MeV energy range. Table 17 presents the radioactive isotopes which produce more than 90 percent of the gamma photons at various times after shutdown. The neutron transmutation reactions and threshold energies of the initial stable isotopes and the resulting radioactive isotopes of Table 17 are found in Table 18. Therefore, to reduce the dose rates significantly, the large component of high energy neutrons must be reduced below the neutron threshold values prior to their interaction with the first wall. An ISSEC (Internal Spectral Shifter and Energy Convertor) structure placed inside the target chamber would be suited for this purpose and its effect on the chamber wall dose rates is presented in Section 3.3.

Table 17. Important Gamma-Photon Producing Isotopes

Chamber Wall: 2-1/4 Cr-1 Mo Steel

Time 0	1 day	1 week	1 month	1 year
Al-28	Cr-51	Cr-51	Cr-51	Mn-54
Cr-51	Mn-54	Mn-54	Mn-54	
V-52	Fe-59	Fe-59	Fe-59	
Mn-54				
Mn-56				
Fe-59				

Chamber Wall: Aluminum-6061-T6

Time 0	1 day	1 week	1 month	1 year
Na-24	Na-24	Cr-51	Cr-51	Mn-54
Mg-27		Mn-54	Mn-54	
Al-28				

Borated Water Shield

Time 0	1 day	1 week	1 month	1 year
N-16	---	---	---	---

Table 18. Neutron Transmutation Reactions Leading to the Radioactive Isotopes in Table 17

2-1/4 Cr-1 Mo Steel Chamber Wall

Reaction(s)	Decay Mode	Threshold Energy (Ref. 17)
$^{28}_{14}Si(n,p)\ ^{28}_{13}Al$	β^-	4.0 MeV (n,p)
$^{52}_{24}Cr(n,p)\ ^{52}_{23}V$	β^-	3.3 MeV (n,p)
$^{52}_{24}Cr(n,2n)\ ^{51}_{24}Cr$	EC	12.3 MeV (n,2n)
$^{53}_{24}Cr^{(n,d)}_{(n,n')p}\ ^{52}_{23}V$	β^-	9.1 MeV (n,d)
$^{54}_{26}Fe(n,\gamma)\ ^{55}_{26}Fe \rightarrow EC \rightarrow\ ^{55}_{25}Mn(n,2n)\ ^{54}_{25}Mn$	EC	10.4 MeV (n,2n)
$^{56}_{26}Fe(n,t)\ ^{54}_{25}Mn$	EC	12.1 MeV (n,t)
$^{56}_{26}Fe(n,p)\ ^{56}_{25}Mn$	β^-	3.0 MeV (n,p)
$^{57}_{26}Fe^{(n,d)}_{(n,n')p}\ ^{56}_{25}Mn$	β^-	8.5 MeV (n,d)
$^{57}_{26}Fe(n,\gamma)\ ^{58}_{26}Fe \rightarrow\ ^{58}_{26}Fe(n,\gamma)\ ^{59}_{26}Fe$	β^-	---
$^{58}_{26}Fe(n,t)\ ^{56}_{25}Mn$	β^-	12.3 MeV (n,t)

Isotope	Primary Gamma (Ref. 15) Energy (MeV)	Secondary Gamma Energy (MeV)
$^{28}_{13}Al$	1.78	---
$^{52}_{23}V$	1.43	---
$^{51}_{24}Cr$	0.325	0.7
$^{54}_{25}Mn$	0.836	---
$^{56}_{25}Mn$	0.845	1.81
$^{59}_{26}Fe$	1.29	1.10

Aluminum-6061-T6 Chamber Wall

Reaction	Decay Mode	Threshold Energy
$^{24}_{12}Mg(n,p)\ ^{24}_{11}Na$	β^-	4.9 MeV (n,p)
$^{26}_{12}Mg(n,\gamma)\ ^{27}_{12}Mg$	β^-	---
$^{27}_{13}Al(n,p)\ ^{27}_{12}Mg$	β^-	1.9 MeV (n,p)
$^{27}_{13}Al(n,\alpha)\ ^{24}_{11}Na$	β^-	3.3 MeV (n,α)
$^{27}_{13}Al(n,\gamma)\ ^{28}_{13}Al$	β^-	---
$^{28}_{14}Si(n,p)\ ^{28}_{13}Al$	β^-	4.0 MeV (n,p)
$^{52}_{24}Cr(n,2n)\ ^{51}_{24}Cr$	EC	12.3 MeV (n,2n)
$^{56}_{26}Fe(n,t)\ ^{54}_{25}Mn$	EC	12.1 MeV (n,t)

Isotope	Primary Gamma Energy (MeV)	Secondary Gamma Energy (MeV)
$^{24}_{11}Na$	2.75	1.37
$^{27}_{12}Mg$	0.84	1.01
$^{28}_{13}Al$	1.78	---
$^{51}_{24}Cr$	0.325	0.7
$^{54}_{25}Mn$	0.836	---

Borated Water Shield

Reaction	Decay Mode	Threshold Energy
$^{16}_{8}O(n,p)\ ^{16}_{7}N$	β^-	10.2 MeV (n,p)

Isotope	Primary Gamma Energy (MeV)	Secondary Gamma Energy (MeV)
$^{16}_{7}N$	6.13	7.11

Since the dose rates at the outer surface of the first wall are considerably higher at 1 day and 1 week after shutdown than is envisioned for routine maintenance of the target chamber, the borated water pool design would need to allow for the drainage of the pool and the assembly of a shadow shield. In particular, access to the ion diodes 1 day after shutdown of the facility is important. Thus, calculations have been performed to compute the lead thickness required to reduce the dose rate to 2.4 mrem/hr. The dose rate within a lead shield as a function of the distance from the outer surface of the steel and aluminum chamber walls is shown in Fig. 21. For the steel chamber wall a thickness of 11.2 cm is required and for the aluminum chamber wall, a thickness of 21 cm.

The alternative TDF design has the target chamber surrounded by a permanent concrete shield. The dose rate within the concrete shield as a function of the distance from the outer surface of the first wall is given in Fig. 22. A concrete thickness of 233 cm for the aluminum chamber and a concrete thickness of 244 cm for the steel chamber are required to reduce the dose rate to 2.4 mrem/hr at shutdown.

Since the concrete shield is a permanent structure, the constituents of the concrete become radioactive thereby producing gamma photon sources within the shield. This accounts for the qualitative difference in the shape of the curves in Fig. 22 as compared to the purely gamma photon attenuation curves of Figs. 19-21.

Another quantity of interest is the primary dose (defined as the neutron and prompt gamma photon dose received directly from the target explosion) received per shot by a person standing next to the edge of the shield. Table 19 presents the primary doses received for aluminum and steel in combination with

Table 19. Primary Dose (mrem/shot)

First Wall + Shield	Gamma Dose	Neutron Dose	Total Dose
Aluminum + Borated Water	2.6×10^{-5}	1.1×10^{-8}	2.6×10^{-5}
Steel + Borated Water	3.2×10^{-5}	2.5×10^{-8}	3.2×10^{-5}
Aluminum + Concrete + Boron	6.6×10^{-7}	1.0×10^{-4}	1.0×10^{-4}
Steel + Concrete + Boron	1.1×10^{-6}	2.1×10^{-4}	2.1×10^{-4}

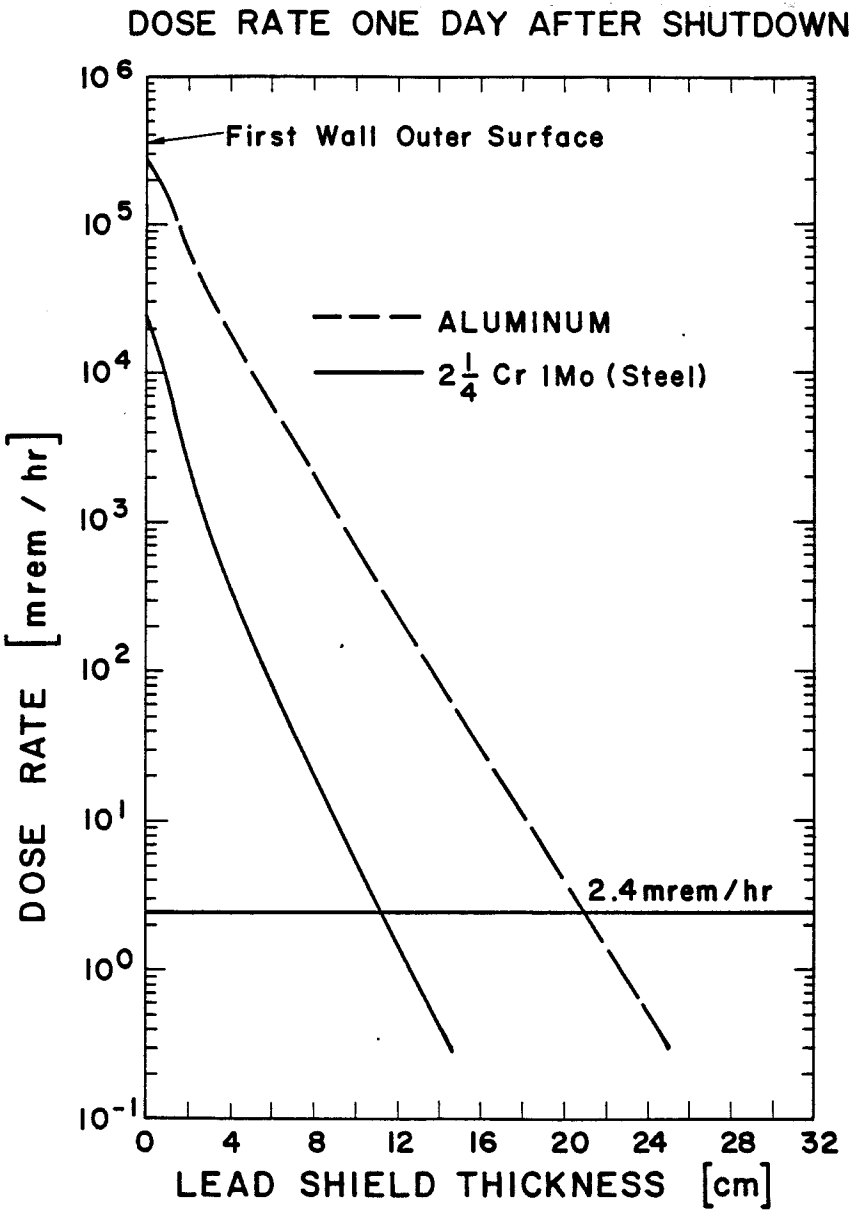

Fig. 21. Dose rate within the lead shield versus distance from outer surface of the aluminum and steel chamber walls 1 day after shutdown.

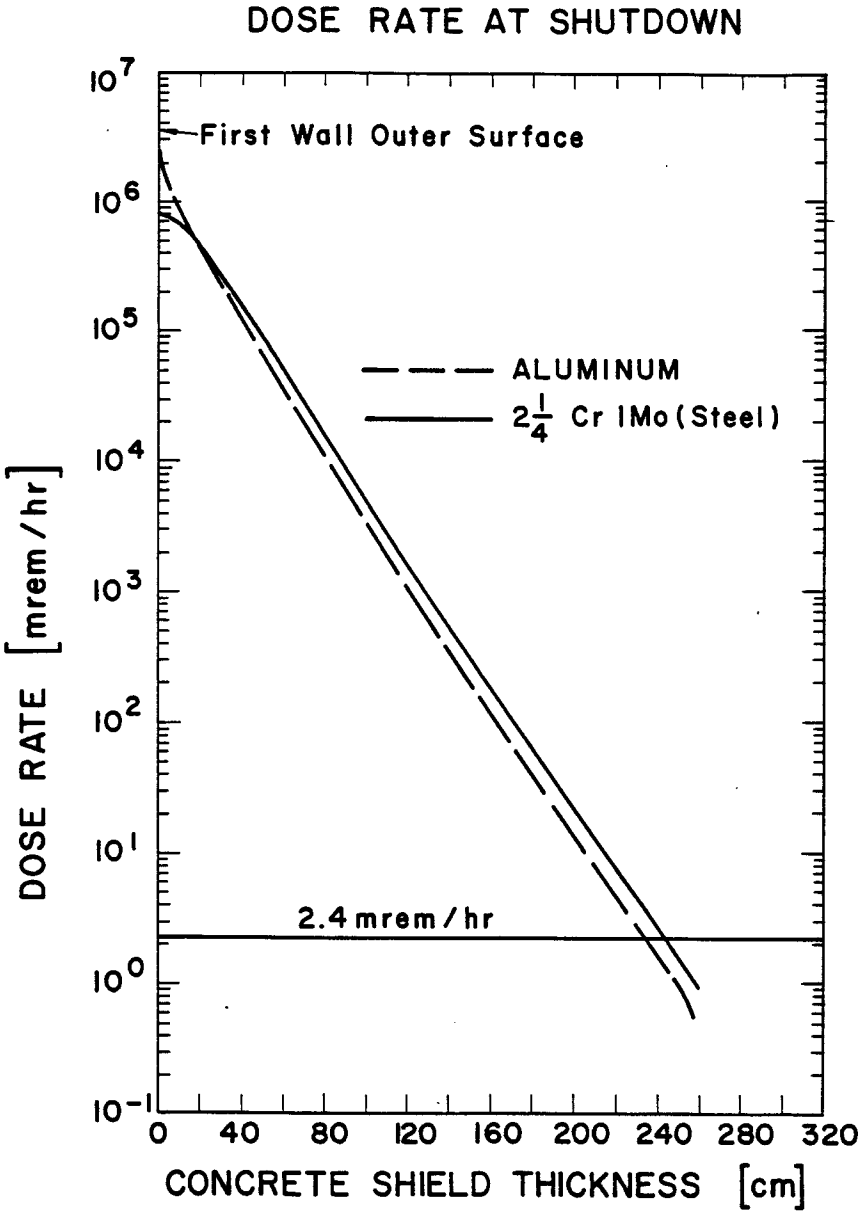

Fig. 22. Dose rate within the concrete shield vs. distance from outer surface of the aluminum and steel chamber walls at shutdown.

either the borated water or concrete shield. As seen, the total dose values computed range from 2.6×10^{-5} mrem/shot for the aluminum chamber wall with borated water shield to 2.1×10^{-4} mrem/shot for the steel chamber wall with concrete shield. Using our assumption of 3120 shots per year, the primary dose is seen to be considerably lower than the dose received from the activated chamber wall, shield and target materials.

3.3 ISSEC Structure and Chamber Wall Analysis

In the previous section it was noted that the chamber wall dose rates are mainly the result of neutron transmutation reactions above neutron threshold values in the MeV energy range (see Table 18). This should not be surprising as over 81% of the source neutrons are above 10 MeV. Hence, to have any impact on the chamber wall dose rates, the large component of high energy neutrons must be softened to below the transmutation threshold values. To achieve this, two ISSEC structures, one made of H-451 graphite and the other of titanium hydride, are considered with each of the chamber wall materials. Figure 7 displays a one-dimensional schematic of the aluminum chamber with the ISSEC structure, boral sheets, and borated water shield used for the neutronics and activation calculations. Figure 8 shows a cut view of the target chamber with the graphite ISSEC.

Figure 23 displays the neutron group flux spectrum within the first mesh cell of the aluminum chamber wall for the ISSEC structures considered. Table 20 gives the corresponding group structure for the flux spectra plotted in Fig. 23. For all of the ISSEC structures considered, the high energy neutron component is reduced. The best result is achieved with the 40% porosity graphite ISSEC structure.

Table 20. Neutron 25 Energy Group Structure in eV Group Limits

Group	E (Top)	E (Low)	E (Midpoint)
1	1.4918 (+7)	1.3499 (+7)	1.4208 (+7)
2	1.3499 (+7)	1.2214 (+7)	1.2856 (+7)
3	1.2214 (+7)	1.1052 (+7)	1.1633 (+7)
4	1.1052 (+7)	1.0000 (+7)	1.0526 (+7)
5	1.0000 (+7)	9.0484 (+6)	9.5242 (+6)
6	9.0484 (+6)	8.1873 (+6)	8.6178 (+6)
7	8.1873 (+6)	7.4082 (+6)	7.7979 (+6)
8	7.4082 (+6)	6.7032 (+6)	7.0557 (+6)
9	6.7032 (+6)	6.0653 (+6)	6.3843 (+6)
10	6.0653 (+6)	5.4881 (+6)	5.7787 (+6)
11	5.4881 (+6)	4.4933 (+6)	4.9907 (+6)
12	4.4933 (+6)	3.6788 (+6)	4.0860 (+6)
13	3.6788 (+6)	3.0119 (+6)	3.3453 (+6)
14	3.0119 (+6)	2.4660 (+6)	2.7390 (+6)
15	2.4660 (+6)	1.3534 (+6)	1.9097 (+6)
16	1.3534 (+6)	7.4274 (+5)	1.0481 (+6)
17	7.4274 (+5)	4.0762 (+5)	5.7518 (+5)
18	4.0762 (+5)	1.6573 (+5)	2.8667 (+5)
19	1.6573 (+5)	3.1828 (+4)	9.8779 (+4)
20	3.1828 (+4)	3.3546 (+3)	1.7591 (+4)
21	3.3546 (+3)	3.5358 (+2)	1.8541 (+3)
22	3.5358 (+2)	3.7267 (+1)	1.9542 (+2)
23	3.7267 (+1)	3.9279 (+0)	2.0597 (+1)
24	3.9279 (+0)	4.1399 (-1)	2.1718 (+0)
25	4.1399 (-1)	2.200 (-2)	2.1800 (-1)

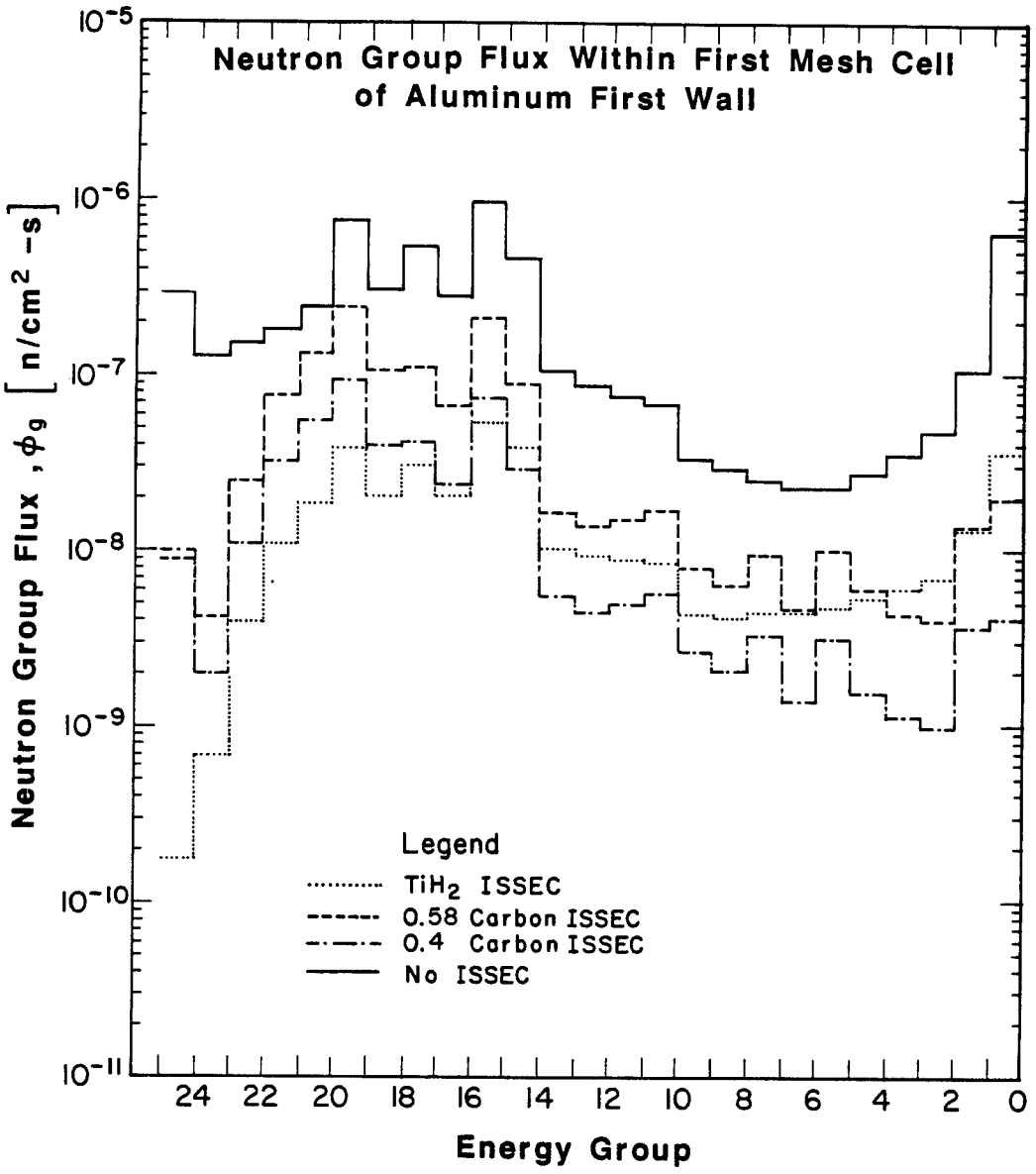

Fig. 23. Neutron group flux within first mesh cell of the aluminum chamber wall.

For the following comparisons, the outer surface of the second boral zone for the ISSEC structure cases corresponds approximately to the first wall outer surface (bare first wall) and will be referred to as the first wall outer surface. Also, the ISSEC structure outer surface will be referred to as the first wall inner surface as they correspond approximately to the same position. The ISSEC structure inner surface has no equivalent in the bare first wall cases, thus it will be referred to as the ISSEC inner surface. The target debris is not included in this analysis.

Table 21 presents a comparison of the dose rates for the aluminum chamber wall with and without the presence of the 40% porosity graphite ISSEC structure. As the comparison shows, the decrease in the dose rate due to the presence of the ISSEC structure is approximately a factor of 1000 at the first wall inner surface and a factor of 100 at the first wall outer surface. Noticeable for the ISSEC structure values, is the large drop in the dose rates to more tolerable levels over the 1 day to 1 week time period after shutdown with the dose rates being 4050 mrem/hr and 13.1 mrem/hr, respectively. This is due to the decay of the $^{24}_{11}Na$ radionuclide which has a half life of 15 hours. The lowest dose rate values are achieved at the ISSEC inner surface. This is a result of both the low activation of the graphite and its impurities and also the attenuation of the aluminum chamber wall gamma photons as they pass through the ISSEC structure.

Figure 24 is a plot of the fractional contribution to the total dose rate for several major contributing isotopes versus time after shutdown for the aluminum chamber wall with the 40% porosity graphite ISSEC structure. Noticeable is the sharp drop in the $^{24}_{11}Na$ contribution beginning at 5 days after shutdown. At 1 week after shutdown the total dose rate has dropped to 13.1

Table 21. Dose Rate Comparison Between Bare Aluminum First Wall and Aluminum Chamber With 40% Porosity Graphite ISSEC

Dose Rates (mrem/hr)

Time After Shutdown	ISSEC* Inner Surface	ISSEC* Outer Surface	Inner+ Surface of First Wall	Outer* Surface of Second Boral Zone	Outer+ Surface Of First Wall
At shutdown	3.54×10^3	8.06×10^4	(6.44×10^6)	3.81×10^4	(2.75×10^6)
1 min	2.87×10^3	6.73×10^4	---	3.14×10^4	---
10 min	1.01×10^3	3.09×10^4	---	1.56×10^4	---
1 hr	7.37×10^2	2.40×10^4	---	1.23×10^4	---
6 hr	5.76×10^2	1.86×10^4	---	9.46×10^3	---
1 day	2.51×10^2	7.98×10^3	(1.12×10^6)	4.05×10^3	(3.61×10^5)
1 week	3.80	25.2	(4.26×10^3)	13.1	(1.29×10^3)
1 month	2.47	12.7	(2.48×10^3)	6.67	(7.18×10^2)
1 year	0.24	4.61	(1.02×10^3)	2.44	(2.84×10^2)

*TDF chamber with graphite ISSEC (0.4 void fraction)

+TDF chamber without ISSEC

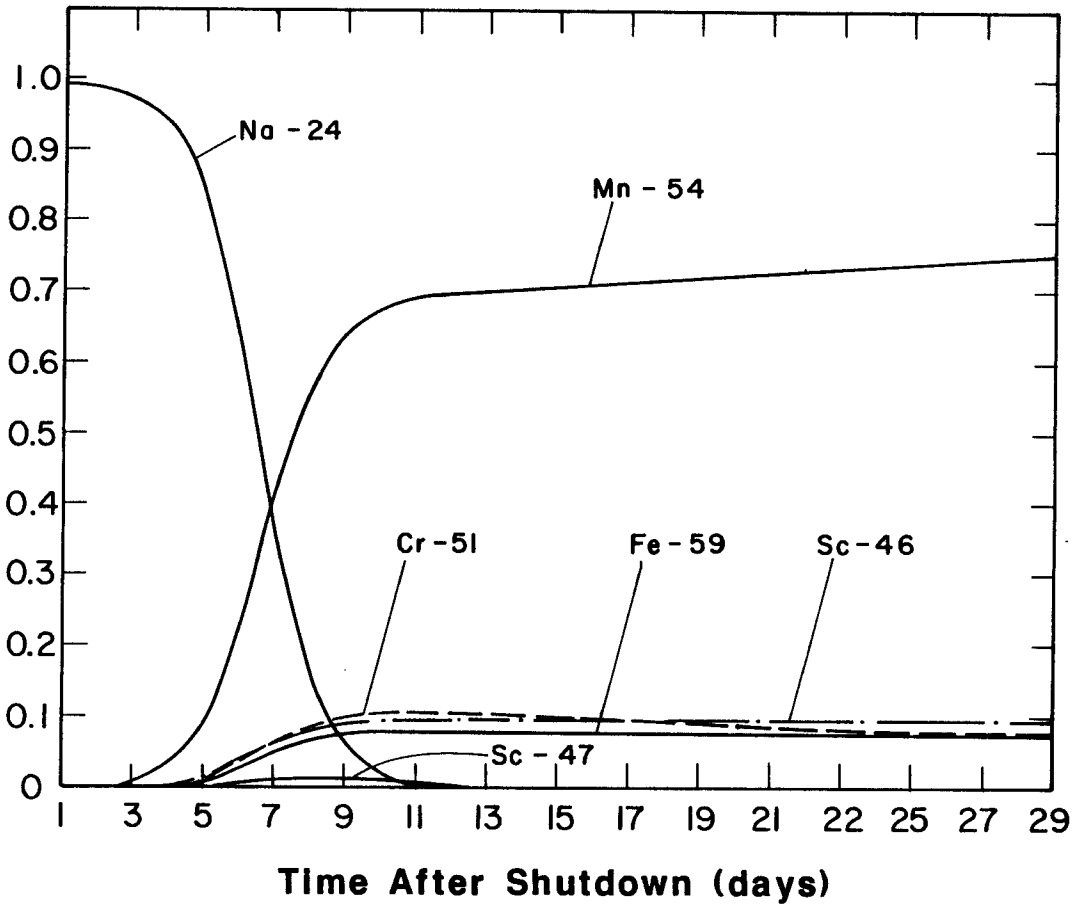

Fig. 24. Fractional contribution to the total dose rate for several major contributing isotopes for the TDF aluminum chamber with 40% porosity carbon ISSEC after 1 year of operation.

mrem/hr (see Table 21) with $^{24}_{11}Na$ and $^{54}_{25}Mn$ having equal contributions. As the $^{24}_{11}Na$ radionuclide decays away the $^{54}_{25}Mn$ radionuclide begins to dominate the total dose. At 29 days after shutdown, its contribution to the total dose rate is approximately 75%. As the shutdown time increases, its dominance steadily increases until at 1 year after shutdown, its dominance is above 96%. Thus, the two major contributing isotopes to the dose rate for this case are $^{24}_{11}Na$ and $^{54}_{25}Mn$.

The comparison of the steel chamber wall dose rates for the cases with and without the presence of the 40% porosity graphite ISSEC structure is given in Table 22. Here the reduction in the first wall outer surface and inner surface dose rate values is not quite as large as with the aluminum chamber wall. The dose rates are reduced by a factor of 25 to 130 at the first wall outer surface. Even though the dose rates are reduced they do not drop to any manageable levels as in the case of the aluminum chamber wall. As with the aluminum chamber wall, the lowest dose rate value for a given time after shutdown occurs at the ISSEC inner surface and is due to the low activation of the ISSEC structure and the attenuation of the chamber wall gamma photons as they pass through the ISSEC structure.

Presented in Table 23 is the dose rate of the aluminum chamber wall with and without the TiH_2 ISSEC structure present. At the first wall's inner and outer surfaces, the reduction in the dose rates is approximately a factor of 20 at shutdown and a factor of 10 at 1 day after shutdown. At 1 week and 1 month after shutdown the ISSEC values actually exceed the bare chamber wall values. The dose rate values become comparable at 1 year after shutdown. One also notices that the dose rate values at the ISSEC structure's inner surface are larger than at the ISSEC structure's outer surface.

Table 22. Dose Rate Comparison Between Bare Ferritic Steel First Wall and Ferritic Steel Chamber With 40% Porosity Graphite ISSEC

Dose Rates (mrem/hr)

Time After Shutdown	ISSEC* Inner Surface	ISSEC* Outer Surface	Inner+ Surface of First Wall	Outer* Surface of Second Boral Zone	Outer+ Surface Of First Wall
At shutdown	2.44×10^3	3.39×10^4	(8.54×10^5)	1.51×10^4	(6.69×10^5)
1 min	1.89×10^3	2.82×10^4	---	1.20×10^4	---
10 min	4.52×10^2	1.37×10^4	---	9.09×10^3	---
1 hr	2.39×10^2	1.04×10^4	---	7.30×10^3	---
6 hr	1.48×10^2	5.77×10^3	---	3.82×10^3	---
1 day	59.6	2.23×10^3	(6.39×10^4)	1.44×10^3	(3.82×10^4)
1 week	6.45	4.38×10^2	(5.96×10^4)	3.43×10^2	(3.54×10^4)
1 month	5.05	3.91×10^2	(5.22×10^4)	3.10×10^2	(2.94×10^4)
1 year	1.28	1.67×10^2	(1.98×10^4)	1.37×10^2	(8.90×10^3)

*TDF chamber with graphite ISSEC (0.4 void fraction)

+TDF chamber without ISSEC

Table 23. Dose Rate Comparison Between Bare Aluminum First Wall and Aluminum Chamber With Titanium Hydride ISSEC

Dose Rates (mrem/hr)

Time After Shutdown	ISSEC* Inner Surface	ISSEC* Outer Surface	Inner+ Surface of First Wall	Outer* Surface of Second Boral Zone	Outer+ Surface Of First Wall
At shutdown	1.15×10^6	2.95×10^5	(6.44×10^6)	1.03×10^5	(2.75×10^6)
1 min	1.14×10^6	2.90×10^5	---	9.30×10^4	---
10 min	1.12×10^6	2.74×10^5	---	8.31×10^4	---
1 hr	1.11×10^6	2.56×10^5	---	7.32×10^4	---
6 hr	1.04×10^6	2.24×10^5	---	5.90×10^4	---
1 day	8.36×10^5	1.50×10^5	(1.12×10^6)	2.83×10^4	(3.61×10^5)
1 week	2.96×10^5	4.06×10^4	(4.26×10^3)	2.17×10^3	(1.29×10^3)
1 month	1.93×10^5	2.67×10^4	(2.48×10^3)	1.40×10^3	(7.18×10^2)
1 year	1.21×10^4	1.69×10^3	(1.02×10^3)	1.01×10^2	(2.84×10^2)

*TDF chamber with TiH_2 ISSEC (0.95 * TiH_2 + 0.5 * Aluminum) having 0.1 void fraction

+TDF chamber without ISSEC

For the TiH_2 ISSEC-steel chamber wall cases presented in Table 24, the dose rate values computed with the TiH_2 ISSEC present do not qualitatively improve the bare steel first wall values. At the first wall inner surface 1 day after shutdown the dose rate of the ISSEC structure case exceeds that of the bare steel wall case. Also, as in the aluminum chamber wall-TiH_2 ISSEC case, the dose rate at the ISSEC inner surface is larger than at the first wall inner surface.

The performance for the TiH_2 ISSEC structure is primarily due to the activation of the ISSEC structure itself (neutron reactions with the titanium isotopes leading to activation products). This is clearly seen by the high dose rates at the ISSEC structure's inner surface as compared to the 40% porosity graphite ISSEC structure values and by the small decrease and even increase in the dose rates at the other positions.

Hence, for the two ISSEC structures considered, the graphite ISSEC clearly is the superior design. The dose rates are lowered and for the aluminum chamber wall, the dose rate is lowered to a more manageable level of 13.1 mrem/hr at 1 week after shutdown. Another positive aspect of the graphite ISSEC is its low activation which greatly contributes to the very low dose rate values at the ISSEC inner surface.

The best combination of target chamber wall material and ISSEC structure shown above is the aluminum chamber wall with the 40% porosity graphite ISSEC structure. This porosity of carbon leads to a dose rate value of 13.1 mrem/hr at 1 week after shutdown. For the design of the facility, it was felt that one could tolerate a dose rate of 50 mrem/hr at 1 week after shutdown. It was estimated that a 58% porosity graphite ISSEC structure would lead to this dose rate value. Table 25 presents a comparison between the 40% porosity and 58%

Table 24. Dose Rate Comparison Between Bare Ferritic Steel First Wall and Ferritic Steel Chamber With Titanium Hydride ISSEC

Dose Rates (mrem/hr)

Time After Shutdown	ISSEC* Inner Surface	ISSEC* Outer Surface	Inner+ Surface of First Wall	Outer* Surface of Second Boral Zone	Outer+ Surface Of First Wall
At shutdown	1.23×10^5	2.15×10^5	(8.54×10^5)	7.42×10^4	(6.69×10^5)
1 min	1.22×10^6	2.11×10^5	---	5.77×10^4	---
10 min	1.20×10^6	2.04×10^5	---	5.37×10^4	---
1 hr	1.17×10^6	1.93×10^5	---	4.73×10^4	---
6 hr	1.05×10^6	1.63×10^5	---	3.27×10^4	---
1 day	8.39×10^5	1.21×10^5	(6.39×10^4)	1.88×10^4	(3.82×10^4)
1 week	3.02×10^5	4.20×10^4	(5.96×10^4)	5.41×10^3	(3.54×10^4)
1 month	1.99×10^5	2.81×10^4	(5.22×10^4)	3.90×10^3	(2.94×10^4)
1 year	1.44×10^4	2.48×10^3	(1.98×10^4)	7.46×10^2	(8.90×10^3)

*TDF chamber with TiH_2 ISSEC (0.95 * TiH_2 + 0.05 * Steel) having 0.1 void fraction

+TDF chamber without ISSEC

Table 25. Dose Rate Comparison Between Aluminum Chamber Containing a 40% Porosity Graphite ISSEC and Aluminum Chamber Containing a 58% Porosity Graphite ISSEC

Dose Rates (mrem/hr)

Time After Shutdown	ISSEC Inner Surface[+]		ISSEC Outer Surface		Outer Surface of Second Boral Zone	
At shutdown	3.54×10^3	(1.72×10^4)	8.06×10^4	(1.95×10^5)	3.81×10^4	(9.77×10^4)
1 min	2.87×10^3	(1.54×10^4)	6.73×10^4	(1.76×10^5)	3.14×10^4	(8.46×10^4)
10 min	1.01×10^3	(1.10×10^4)	3.09×10^4	(1.20×10^5)	1.56×10^4	(5.84×10^4)
1 hr	7.37×10^2	(9.70×10^3)	2.40×10^4	(9.92×10^4)	1.23×10^4	(4.88×10^4)
6 hr	5.76×10^2	(7.61×10^3)	1.86×10^4	(7.75×10^4)	9.46×10^3)	(3.79×10^4)
1 day	2.51×10^2	(3.30×10^3)	7.98×10^3	(3.35×10^4)	4.05×10^3	(1.63×10^4)
1 week	3.80	(8.75)	25.2	(1.00×10^2)	13.1	(49.7)
1 month	2.47	(3.59)	12.7	(50.1)	6.67	(25.2)
1 year	0.24	(0.97)	4.61	(20.0)	2.44	(10.0)

[+]Values enclosed by ( ) are for a graphite ISSEC having 0.58 void fraction

Values not enclosed are for a graphite ISSEC having 0.4 void fraction

porosity graphite ISSEC structures. At the outer surface of the second boral zone a dose rate of 49.7 mrem/hr at 1 week after shutdown was achieved for the 58% porosity graphite ISSEC. The large drop in the dose rates for the period 1 day to 1 week after shutdown is still apparent with the magnitude of the values being approximately a factor of 4 higher than the 40% porosity ISSEC. The dose rates are still considerably reduced from the original bare aluminum chamber wall values (see Table 21), particularly for the period of 1 day after shutdown.

For the aluminum chamber wall-graphite ISSEC results, a plot, Fig. 25, of the dose rate at 1 day and 1 week after shutdown versus the porosity of a 1 meter thick graphite ISSEC structure was made by extrapolating the results obtained from the two point design calculations. The bare aluminum chamber wall cases are indicated and correspond to 100% porosity. A rough estimate of the dose rates at the first wall outer surface at 1 day and 1 week after shutdown for a graphite ISSEC structure of an arbitrary porosity can now be obtained.

As a summary to this section, three graphs comparing the results of the two ISSEC structures in combination with either chamber wall material are shown in Figs. 26-28. Figure 26 displays the first wall outer surface results; Fig. 27, the ISSEC outer surface results; and Fig. 28, the ISSEC inner surface results. The superiority of the graphite ISSEC structure over the TiH_2 ISSEC structure is clearly discernible. Also noticeable is the large drop in the dose rate values between 1 day and 1 week after shutdown for both of the graphite ISSEC-aluminum chamber wall cases. As was shown in Fig. 24, this is primarily the result of the decay of the $^{24}_{11}Na$ radionuclide.

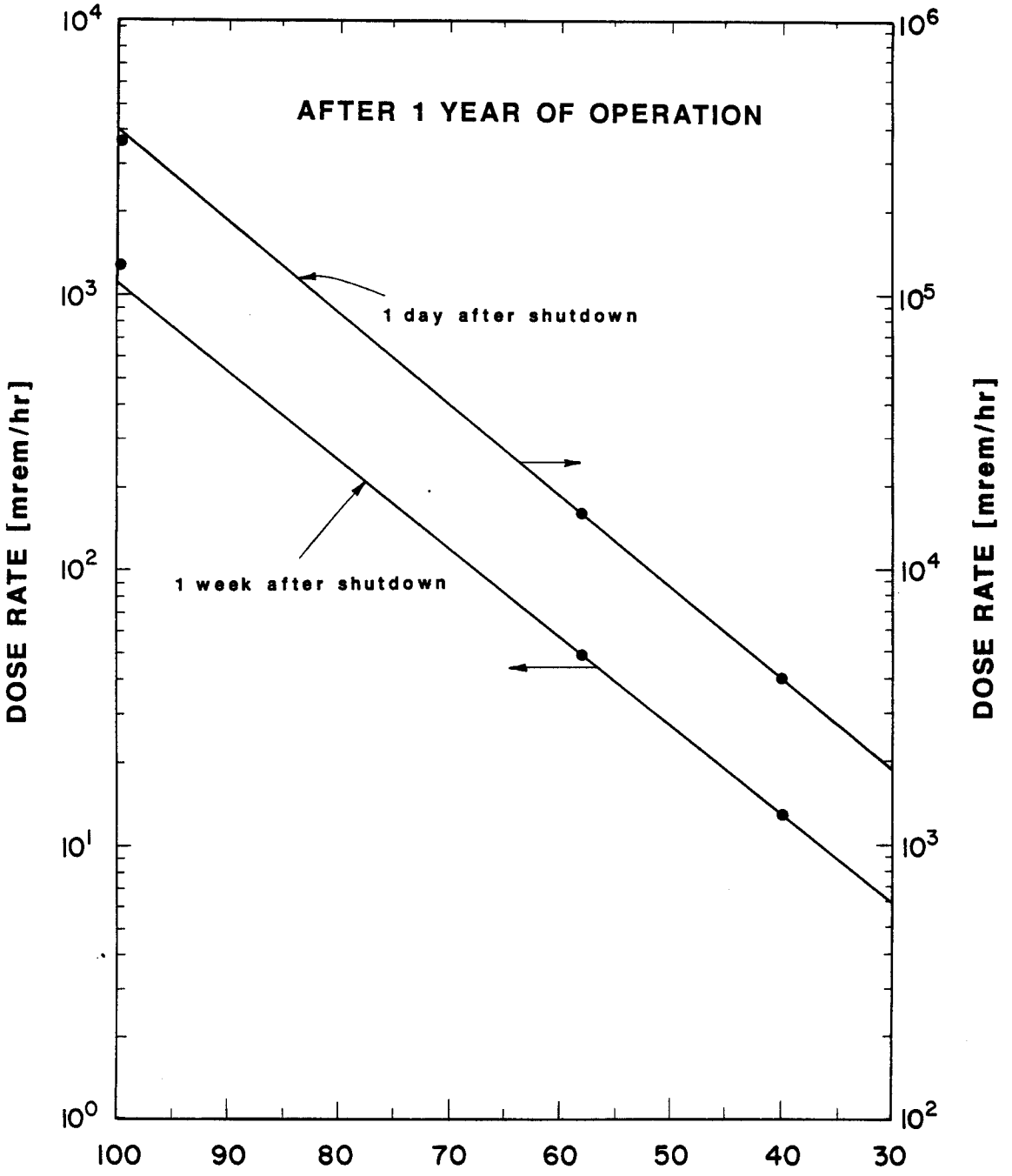

Fig. 25. Dose rate versus porosity of carbon ISSEC in a 1 meter thickness zone.

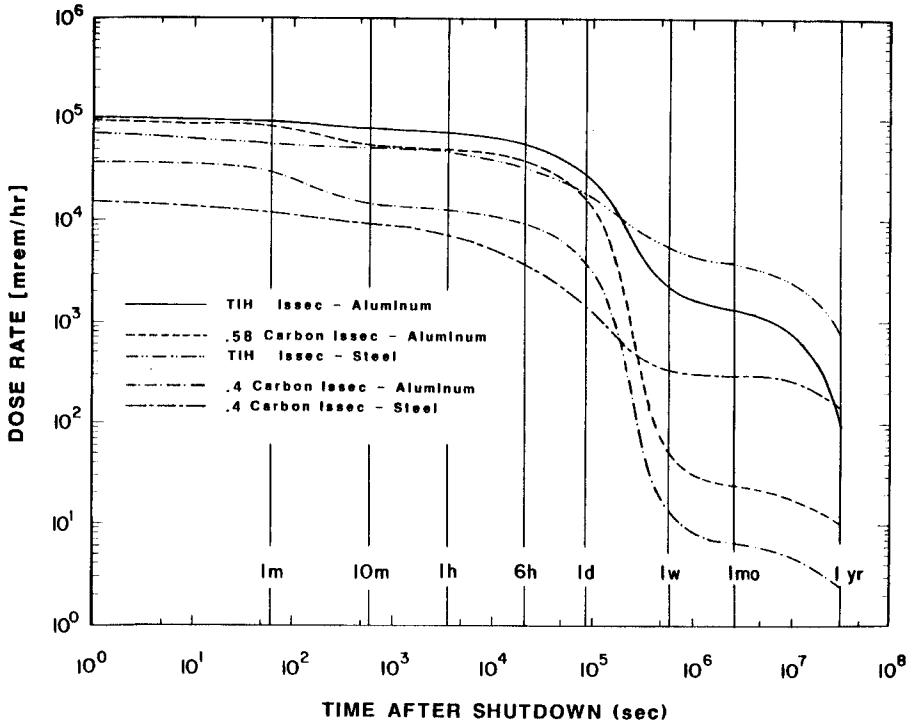

Fig. 26. Dose rate at the chamber wall outer surface versus time after shutdown for the 5 different design cases involving ISSEC structures.

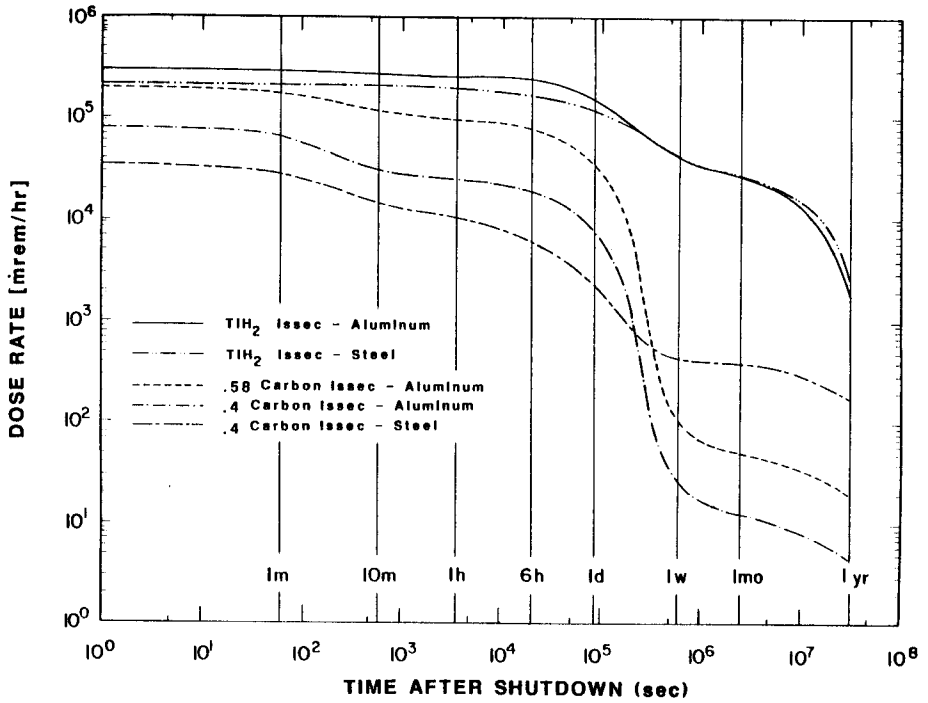

Fig. 27. Dose rate at the chamber wall inner surface versus time after shutdown for the 5 different design cases involving ISSEC structures.

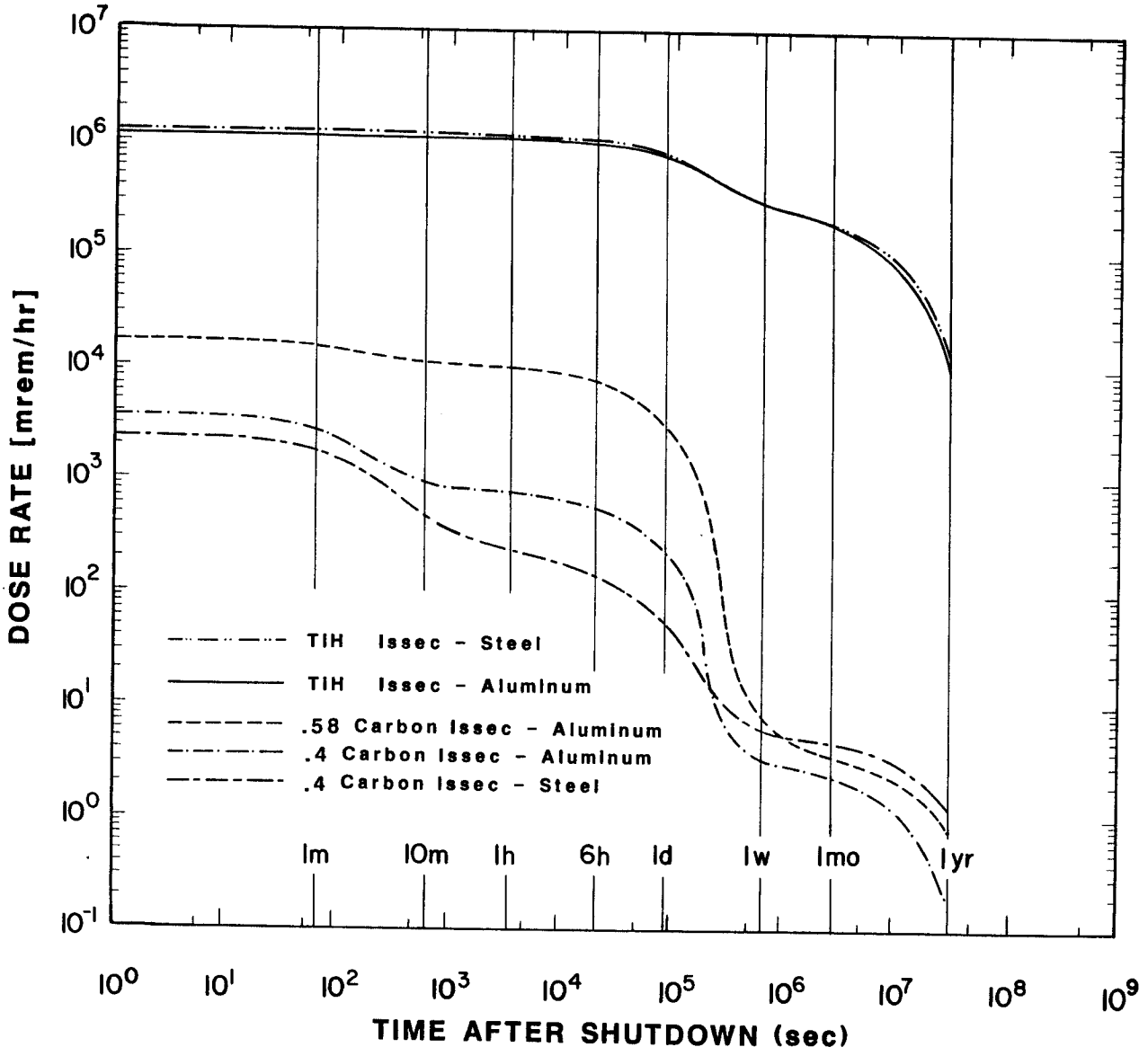

Fig. 28. Dose rate at the ISSEC inner surface versus time after shutdown for the 5 different design cases involving ISSEC structures.

3.4 Maintenance Schedule

In the previous section it was shown that the aluminum chamber wall with the 40% porosity graphite ISSEC had the lowest value for the dose rate at the first wall outer surface at 1 week after shutdown. This case will serve as the basis for the definition of a maintenance schedule.

As the Target Development Facility is an experimental facility, access to the ion diodes relatively soon after the last shot is important. Thus it is essential that one has a more detailed knowledge of the dose rates for the first several days after shutdown of the facility. In particular, it is of interest to determine at what time after shutdown the large drop in the dose rate occurs. Table 26 presents the dose rate at half day intervals for the time period 1 day through 1 week. Beginning at 1 day after shutdown, the dose rate drops approximately by a factor of 1.74 each half day period until 4 days after shutdown. It is to be remembered, that during this time period the $^{24}_{11}Na$ radionuclide dominates the total dose rate.

Using the information presented in Table 26 and having identified the major contributors to the dose rate between 1 day and 1 week after shutdown (see Fig. 24), the total integrated dose that a person would obtain working in this radiation environment is calculated. The maintenance schedules presented are based on the following criteria: 5 rem per year; an average of 1.25 rem per quarter; 3 rem for the worst quarter with an average of 2/3 rem per quarter available for the remaining 3 quarters, 13 weeks per quarter. The position chosen was the outer surface of the second boral zone (see Fig. 7). Two maintenance schedules are suggested: the first has the maintenance period as 2 days for which a worker would be working 8 hours per day and the second has a 12 hour continuous working period.

Table 26. Dose Rates for Aluminum Chamber With 40% Porosity Graphite ISSEC at Half Day Intervals

Dose Rates (mrem/hr)

Time After Shutdown	ISSEC Inner Surface	ISSEC Outer Surface	Outer Surface Second Boral
At shutdown	3.54×10^3	8.06×10^4	3.81×10^4
1 day	2.51×10^2	7.98×10^3	4.05×10^3
1.5 days	1.46×10^2	4.58×10^3	2.33×10^3
2 days	85.7	2.64×10^3	1.34×10^3
2.5 days	50.9	1.52×10^3	7.72×10^2
3 days	31.0	8.79×10^2	4.46×10^2
3.5 days	19.4	5.11×10^2	2.59×10^2
4 days	12.8	3.00×10^2	1.52×10^2
4.5 days	8.93	1.79×10^2	91.0
5 days	6.68	1.09×10^2	55.7
5.5 days	5.35	69.1	35.4
6 days	4.57	46.1	23.7
6.5 days	4.09	32.8	17.0
1 week	3.80	25.2	13.1

Table 27 presents the 2 day maintenance period working schedule. The schedule is broken up into four different operating + waiting period cycles with the operating period being 4.5 days of testing. As an example of the schedule let's choose the column; operate 4.5 days -- wait 6.5 days. The dose rate at the beginning of the maintenance period (in this case it's after 6.5 days of waiting) is 17.0 mrem/hr and at the end of the second day maintenance period, the dose rate is 9.96 mrem/hr. The integrated dose received during the maintenance period by the worker is 0.207 rem. This is labeled as "Dose received during one work cycle." The number of such operating + working cycles in one quarter year is given in the next row. For our example this is 7.4. The number of cycles a worker can work to receive the average dose of 1.25 rem is 6 cycles (i.e., the worker rests 1 cycle per quarter). To receive a dose of 3 rem, the worker can work 14.5 cycles and to receive 2/3 rem the worker can only work 3.2 cycles. Thus, as one views Table 27, one notices that the column "operate 4.5 days -- wait 6.5 days," has the best match between cycles/quarter and work to receive the average dose of 1.25 rem.

Table 28 has the same format as Table 27 but now the maintenance period is a 12 hour continuous work period. Again comparing cycles per quarter and work to receive the 1.25 rem for each of the four different cycles, one notes again that the column labeled "operate 4.5 days -- wait 6.5 days" has the best match.

Thus, for both schedules, the best match between the number of operating cycles per quarter and cycles of work to receive 1.25 rem was to operate the facility for 4.5 days and to wait 6.5 days.

Several methods to shorten the waiting period can be suggested: (1) shorten the maintenance period; (2) spread out dose among several workers;

Table 27. Maintenance Schedule for the Target Development Facility with Aluminum Chamber with 40% Porosity Graphite ISSEC

Criteria:

1.25 rem per quarter

3 rem for worst quarter

Outer surface of second boral zone

2 days of maintenance work @ 8 hours per day

13 weeks per quarter gives 91 days per quarter

	Operate 4.5 Days Wait 3.5 Days	Operate 4.5 Days Wait 4.5 Days	Operate 4.5 Days Wait 5.5 Days	Operate 4.5 days Wait 6.5 Days
Dose rate at beginning	259 mrem/hr	91.0 mrem/hr	35.4 mrem/hr	17.0 mrem/hr
Dose Rate at end	65.0 mrem/hr	26.7 mrem/hr	14.1 mrem/hr	9.96 mrem/hr
Dose received during one work cycle	2.36 rem	0.861 rem	0.369 rem	0.207 rem
Cycles/quarter	9.75	8.81	8.03	7.38
Work to receive 1.25 rem	0.53 cycles	1.45 cycles	3.39 cycles	6.04 cycles
Work to receive 3 rem	1.27 cycles	3.48 cycles	8.13 cycles	14.49 cycles
Work to receive 0.67 rem	0.28 cycles	0.77 cycles	1.81 cycles	3.22 cycles

Table 28. Maintenance Schedule for the Target Development Facility with Aluminum Chamber with 40% Porosity Graphite ISSEC

Criteria:

1.25 rem per quarter

3 rem for worst quarter

Outer surface of second boral zone

1 day of maintenance work for 12 hours

13 weeks per quarter gives 91 days per quarter

	Operate 4.5 Days Wait 3.5 Days	Operate 4.5 Days Wait 4.5 Days	Operate 4.5 Days Wait 5.5 days	Operate 4.5 Days Wait 6.5 Days
Dose rate at beginning	259 mrem/hr	91.0 mrem/hr	35.4 mrem/hr	17.0 mrem/hr
Dose rate at end	152 mrem/hr	55.7 mrem/hr	23.7 mrem/hr	13.1 mrem/hr
Dose received during one work cycle	2.41 rem	0.856 rem	0.346 rem	0.178 rem
Cycles/quarter	10.71	9.58	8.67	7.91
Work to receive 1.25 rem	0.52 cycles	1.46 cycles	3.61 cycles	7.02 cycles
Work to receive 3 rem	1.24 cycles	3.50 cycles	8.67 cycles	16.85 cycles
Work to receive 0.67 rem	0.27 cycles	0.78 cycles	1.93 cycles	3.75 cycles

(3) supply additional shielding, (4) reduce the $^{24}_{11}Na$ dose rate component further since it dominates the dose rate between 1 day and 1 week after shutdown (see Fig. 24).

3.5 Pulse Nature of the Facility

In Section 2.2 it was indicated that the target chamber wall activation and dose rate calculations were preformed assuming a continuous average neutron flux irradiation to the facility. In reality the Target Development Facility will test ten to twelve fusion targets per day at approximately 1 hour intervals. Since DKR is a continuous irradiation code, calculations simulating a given pulse sequence are not possible, but a single pulse can be analyzed. Table 29 presents the results (activity in curies) for the aluminum chamber wall with and without the presence of the 40% porosity graphite ISSEC structure. It is apparent that the short term activity (at shutdown to 10 min after shutdown) is larger for the pulsed case than for the 1 year continuous average irradiation flux. In Tables 30 and 31 some of the contributors to the radioactivity during this period and their activity are listed. The isotopes with half-lives on the order of seconds influence the dose rates at shutdown and those with half-lives on the order of several minutes influence the dose rates up to an hour after shutdown. This difference in the dose rate values is a consequence of the continuous irradiation assumption used by the DKR code which manifests itself in the activity and dose rates of the short-lived isotopes. To understand this more clearly, we examine the pulsed neutron irradiation. During one 200 MJ shot, 7.093×10^{19} neutrons are released. Multiplying this by the number of shots in a year, 3120, and dividing by the number of seconds in a year, 3.156×10^{7}, one arrives at the average continuous irradiation value of 7.012×10^{15} neutron/s. This is 4 orders of magnitude lower

Table 29. Activity Comparison Between the 1 Year Steady State and 1 Pulse Computations for the Bare Aluminum Chamber and the Aluminum Chamber With 40% Porosity Graphite ISSEC

Activity (curies)

	Without ISSEC		With Graphite ISSEC	
Time After Shutdown	(1 yr steady state)	(1 pulse)	(1 yr steady state)	(1 pulse)
At shutdown	5.54×10^{4}	2.66×10^{6}	1.42×10^{3}	6.92×10^{4}
1 min	4.61×10^{4}	1.22×10^{6}	1.16×10^{3}	3.64×10^{4}
10 min	2.15×10^{4}	1.35×10^{5}	4.38×10^{2}	3.78×10^{3}
1 hr	1.44×10^{4}	3.77×10^{3}	2.53×10^{2}	89.6
6 hr	1.12×10^{4}	1.49×10^{3}	1.86×10^{2}	27.7
1 day	4.92×10^{3}	6.12×10^{2}	80.0	9.98
1 week	2.24×10^{2}	1.17	3.85	1.93×10^{-2}
1 month	1.65×10^{2}	0.223	2.79	3.99×10^{-3}
1 year	59.0	2.49×10^{-2}	0.958	4.00×10^{-4}
10 years	3.38	1.22×10^{-3}	6.98×10^{-2}	2.48×10^{-5}
100 years	8.75×10^{-2}	2.83×10^{-5}	1.11×10^{-2}	3.57×10^{-6}
1000 years	1.98×10^{-3}	6.34×10^{-7}	7.31×10^{-3}	2.34×10^{-6}

Table 30. Major Contributors to the Bare Aluminum Chamber Wall Activity for the 1 Year Steady State and 1 Pulse Computations

Important Contributors to the Activity (Curies) (1 yr Average Flux)

Isotope	$t_{1/2}$	At Shutdown	1 min	10 min	1 hr	6 hr
Na-24	15.0 hr+	1.40×10^{4}	1.40×10^{4}	1.39×10^{4}	1.34×10^{4}	1.06×10^{4}
Na-26	1.07 s+	2.70	4×10^{-17}	0	0	0
Mg-27	9.46 min+	1.08×10^{4}	1.00×10^{4}	5.20×10^{3}	1.33×10^{2}	3.8×10^{-8}
Al-28	2.24 min+	2.84×10^{4}	2.09×10^{4}	1.29×10^{3}	2.5×10^{-4}	0
Al-30	3.69 s+	2.63	3.3×10^{-5}	0	0	0
Li-8	8.42 ms	2.13	8×10^{-22}	0	0	0
N-16	7.10 s+	1.00×10^{3}	2.95	5×10^{-23}	0	0
Cu-66	5.11 min+	67.9	59.3	17.5	2.0×10^{-2}	4×10^{-20}

Important Contributors to the Activity (Curies) (1 Pulse)

Isotope	$t_{1/2}$	At Shutdown	1 min	10 min	1 hr	6 hr
Na-24	15.0 hr+	1.82×10^{3}	1.82×10^{3}	1.81×10^{3}	1.74×10^{3}	1.38×10^{3}
Na-26	1.07 s+	1.77×10^{4}	3×10^{-13}	0	0	0
Mg-27	9.46 min+	1.34×10^{5}	1.25×10^{5}	6.45×10^{4}	1.65×10^{3}	4.7×10^{-7}
Al-28	2.24 min+	1.48×10^{6}	1.09×10^{6}	6.72×10^{4}	1.3×10^{-2}	0
Al-30	3.69 s+	5.04×10^{3}	6.3×10^{-2}	0	0	0
Li-8	8.42 ms	1.77×10^{4}	6×10^{-18}	0	0	0
N-16	7.10 s+	9.91×10^{5}	2.91×10^{3}	5×10^{-20}	0	0
Cu-66	5.11 min+	1.55×10^{3}	1.36×10^{3}	4.00×10^{2}	0.454	$1. \times 10^{-18}$

+Gamma-photon producing isotope

Table 31. Major Nuclide Contributors to the Aluminum Chamber With 40% Porosity Graphite ISSEC Activity for the 1 Year Steady State and 1 Pulse Computations

Important Contributors to the Activity (Curies) (1 yr Average Flux)

Isotope	$t_{1/2}$	At Shutdown	1 min	10 min	1 hr	6 hr
Na-24	15.0 hr+	2.20×10^{2}	2.20×10^{2}	2.18×10^{2}	2.10×10^{2}	1.67×10^{2}
Na-26	1.07 s+	1.7×10^{-2}	3×10^{-19}	0	0	0
Mg-27	9.46 min+	2.76×10^{2}	2.56×10^{2}	1.33×10^{2}	3.40	1.0×10^{-9}
Al-28	2.24 min+	8.59×10^{2}	6.31×10^{2}	38.9	7.4×10^{-6}	0
Al-30	3.69 s+	2.5×10^{-2}	3.0×10^{-7}	0	0	0
Li-8	842 ms	1.61	6×10^{-22}	0	0	0
N-16	7.10 s+	7.12	2.1×10^{-2}	3×10^{-25}	0	0
Cu-66	5.11 min+	1.40	1.23	0.362	4.1×10^{-4}	9×10^{-22}

Important Contributors to the Activity (Curies) (1 Pulse)

Isotope	$t_{1/2}$	At Shutdown	1 min	10 min	1 hr	6 hr
Na-24	15.0 hr+	28.6	28.6	28.4	27.3	22.0
Na-26	1.07 s+	1.11×10^{2}	2×10^{-15}	0	0	0
Mg-27	9.46 min+	3.42×10^{3}	3.18×10^{3}	1.65×10^{3}	42.2	1.2×10^{-8}
Al-28	2.24 min+	4.48×10^{4}	3.29×10^{4}	2.03×10^{3}	3.9×10^{-4}	0
Al-30	3.69 s+	31.5	4.0×10^{-4}	0	0	0
Li-8	843 ms	1.34×10^{4}	5×10^{-18}	0	0	0
N-16	7.10 s+	7.04×10^{3}	20.7	3×10^{-22}	0	0
Cu-66	5.11 min+	32.1	28.0	8.27	9.4×10^{-3}	2×10^{-20}

+Gamma-photon producing isotope

than the pulsed value. Hence, the isotopes most affected by the continuous irradiation assumption are the short-lived isotopes which saturate very quickly in the average continuous irradiation flux. Consequently, the dose rate values given at shutdown and 1 min and 10 min after shutdown for the chamber wall and ISSEC structure analysis may be a factor of 10^2 to 10^3 too low at shutdown and 10 to 10^2 too low between 1 min to 10 min after shutdown.

For the aluminum target chamber wall, preliminary calculations indicate that the pulse sequence or operation sequence chosen may influence the dose rate up to 1 week after shutdown of the facility. This is primarily due to the $^{24}_{11}Na$ radionuclide which has a 15 hr half-life and which therefore is sensitive to the pulse sequence used by the facility. Indications are that the dose rate component due to the $^{24}_{11}Na$ radionuclide could increase by nearly a factor of 2 depending on the pulse sequence. Recall that $^{24}_{11}Na$ is the dominant contributor to the dose rate during the period 1 day to 1 week after shutdown (see Fig. 24) and that the maintenance schedule is strongly influenced by dose rates during this period of time. Hence, the pulse sequence or operation sequence for the aluminum target chamber may have some influence on the type of maintenance schedule chosen for the facility. The reverse condition may also hold true.

On the same note, the saturation period for $^{24}_{11}Na$ is approximately 1 week so that any problems associated with $^{24}_{11}Na$ will be present whether the facility operates for 1 week or for 1 year.

In Section 3.2, the dose rate values at shutdown at the edge of the water shield were given as 10.2 mrem/hr and 20.5 mrem/hr for the bare aluminum chamber and steel chamber, respectively. The dose rates at the edge of the shield at shutdown are predominately that due to $^{16}_{7}N$. From Table 30 one notices that

the activity of $^{16}_{7}N$ after one shot is approximately 10^6 curies compared to the continuous irradiation value of 10^3 curies. Hence, the dose rate values given at the edge of the water shield at shutdown in Section 3.2 should read approximately 10^7 mrem/hr for the aluminum chamber and 2×10^7 mrem/hr for the steel chamber. The values given for 1 day after shutdown are not influenced by $^{16}_{7}N$ as the activity becomes negligible 5 to 6 minutes after a shot. The production of $^{16}_{7}N$ amounts to approximately 1.2 curies per liter.

Since $^{16}_{7}N$ is a gas, one becomes concerned over its release into the atmosphere of the building. This depends upon the diffusion or transport of the $^{16}_{7}N$ through the water to the pool surface and subsequently through the atmosphere. Nevertheless a worst case calculation was performed assuming that the $^{16}_{7}N$ instantaneously fills the volume contained by a building 8 m in diameter and 10 m high. The thickness of concrete required to reduce the absorbed dose outside the building to a worker's weekly average was computed to be 185 cm for the 10^6 curies case and 100 cm for the 10^3 curies case. Thus the worst case situation leads to very thick concrete walls. To get a more realistic answer the diffusion rate of the $^{16}_{7}N$ to the surface of the borated water shield needs to be investigated. A total of approximately 2.88×10^{21} atoms of $^{16}_{7}N$ are produced per shot. This is relatively low compared to the total number of water molecules present in the borated water pool. Ways to inhibit the diffusion of $^{16}_{7}N$ into the atmosphere are to have a water jet (water streamer) directed down onto the chamber and/or to cover the pool area with a plexiglas or plastic covering. The diffusion upward need only be inhibited until the activity becomes negligible which is 5 to 6 minutes after shutdown.

4. SUMMARY

Biological dose rates have been determined for the TDF target chamber (with and without an ISSEC structure present) and accumulated target debris after an operational period of 1 year (3120 shots per year). For the case without the ISSEC structure present, it has been shown that at the inner surface of the chamber the dose rate attributed to the target debris can be comparable to the dose rate of the first wall materials depending on the specific target materials used. Even with periodic removal of the thermal liner upon which the radioactive target debris has condensed, the dose rates at the inner surface still remain too high for hands on maintenance. At the outer surface of the first wall the dose rate attributed to the target debris is lower than that of the first wall. Nevertheless, the dose rate at the outer surface is still larger than is acceptable for routine maintenance of the target chamber. The thickness of lead required for use as a shadow shield 1 day after shutdown of the facility has been calculated to be 11.2 cm for 2-1/4 Cr-1 Mo steel chamber and 21 cm for the aluminum chamber. This reduces the dose rate to 2.4 mrem/hr. An alternative design using a permanent concrete shield requires 233 cm of concrete for the aluminum chamber and 244 cm of concrete for the 2-1/4 Cr-1 Mo steel chamber to reduce the dose rate to 2.4 mrem/hr at shutdown. The primary dose at the edge of the shield received from the target explosion has been found to be considerably lower than that due to the activated chamber wall and shield.

The presence of an ISSEC structure was suggested when an examination of the nuclide decay chains given by the DKR code showed that the target chamber wall dose rate is mainly the result of high energy neutron transmutation reactions above neutron threshold values in the MeV energy range. Two ISSEC

structures were examined, one made from graphite and the other from titanium hydride, TiH_2. The graphite ISSEC structure was shown to be superior to the TiH_2 ISSEC as the activation of the graphite structure is low and is mainly the result of its impurities. The TiH_2, on the other hand, was highly activated. The largest reduction in the dose rates, which resulted in dose rates being lowered to tolerable levels (< 50 mrem/hr), was achieved by the aluminum chamber wall with the graphite ISSEC structure. In particular, the 40% graphite ISSEC structure dropped the dose rate at the first wall outer surface to 13.1 mrem/hr at 1 week after shutdown. This is not without its cost, though. The price paid for the reduction in the dose rates is in the amount of mass required for the ISSEC structure. For the 40% porosity graphite, this amounts to approximately 124 metric tons and for the 58% porosity graphite, 87 metric tons. The aluminum chamber wall without support structure has a mass of 71 metric tons.

The maintenance schedules were based upon the aluminum chamber wall and 40% porosity graphite ISSEC structure. For both schedules presented, the best matchup between the number of operating cycles per quarter and cycles of work to receive the average dose of 1.25 rem per quarter was achieved by operating the facility for 4.5 days and waiting for 6.5 days. The long waiting period is necessitated by the high activity of $^{24}_{11}Na$. It is only after its decay to lower levels (approximately after 5 days) that the first wall is more easily accessible.

An examination of the dose rates after a single pulse reveals that the short-lived isotopes, some of which contribute to the dose rate up to 1 hr after shutdown, are affected most by the pulse nature of the facility. For the aluminum target chamber, preliminary calculations indicate that the pulse

sequence or operation sequence chosen for the operation facility may influence the dose rate component attributed to $^{24}_{11}Na$ up to a factor of 2 which in turn would affect the chamber maintenance. On the same note, the saturation period for $^{24}_{11}Na$ is approximately 1 week so that any problems associated with it will be present whether one operates the facility for 1 week or for 1 year.

The target activation analysis has shown that the induced radioactivity of the pusher materials decays within 3 minutes after the target explosion and that the activity can essentially be considered as that from the high-Z tamper material.

Acknowledgement

Support for this work has been provided by Sandia National Laboratories under contract #59-3149. The authors wish to thank Prof. W.F. Vogelsang, Dr. A.M. White, and Prof. S.I. Abdel-Khalik for their helpful discussions.

References

1. K.J. O'Brien, G.A. Moses, A.M. White, "Neutron Activation and Shielding of the Light Ion Fusion Target Development Facility," Nucl. Tech./Fusion 4, 883 (1983).

2. R.O. Bangerter, "Ion Beam Targets, Laser Program Annual Report - 1976," UCRL-50021-76, Lawrence Livermore National Laboratory Report, Section 4.2.

3. D.L. Henderson, A.M. White, G.A. Moses, "Target Material Activation Calculations for High Gain Light Ion Fusion Targets," University of Wisconsin Fusion Technology Institute Report UWFDM-572 (1984).

4. B. Badger et al., "HIBALL - A Conceptual Heavy Ion Beam Driven Reactor Study," University of Wisconsin Fusion Technology Institute Report UWFDM-450, KfK-3202, Part I, Chapter III (1981).

5. R.L. Engelstad, E.G. Lovell, G.A. Moses, "Fatigue Strength Analysis of the Sandia Target Development Facility Reaction Chamber," Sixth Top. Mtg. on the Tech. of Fusion Energy, San Francisco, CA, 3-7 March 1985.

6. R.G. Jaeger et al., Engineering Compendium on Radiation Shielding, Springer-Verlag, New York (1975), Vol. 2, p. 173.

7. Theodore Rockwell, III, Reactor Shielding Design Manual, D. Van Nostrand Company (1956), p. 189.

8. HEDL Reduced Activation Program (Material Presented at the Planning Meeting for Development of Low Activation Austenitic and Ferritic Steels, ORNL, Feb. 7-8, 1984).

9. G.R. Hopkins, R.J. Price, R.E. Bullock, J.A. Dalessandro and N.B. Elsner, "Carbon and Silicon Carbide as First Wall Materials in Inertial Confinement Fusion Reactors," GA-A14894 (March 1978).

10. W. Engles, "A User's Manual for ANISN," RSIC Code Package CCC-254, Radiation Shielding and Information Center, Oak Ridge National Laboratory, Oak Ridge, TN.

11. RSIC Data Library Collection, "Vitamin-C, 171 Neutron, 36 Gamma-Ray Group Cross Section Library in AMPX Interface Format for Fusion Neutronics Studies," DLC-41, ORNL.

12. RSIC Data Library Collection, "MACKLIB-IV, 171 Neutron, 36 Gamma-Ray Group Kerma Factor Library," DLC-60, ORNL.

13. Tak Yun Sung, "DKR: A Radioactivity Calculation Code for Fusion Reactors," University of Wisconsin Fusion Technology Institute Report UWFDM-170 (1976).

14. T.Y. Sung and W.F. Vogelsang, "Decay Chain Data Library for Radioactivity Calculations," University of Wisconsin Fusion Technology Institute Report UWFDM-171 (1976).

15. C.M. Lederer et al., Table of Isotopes, Sixth and Seventh Editions, Wiley (1967 & 1978).

16. M.A. Gordinier and R.J. Howerton, "ACTL: Evaluated Neutron Activation Cross Section Library - Evaluation Techniques and Reaction Index," UCRL-50400, Vol. 18 (1978).

17. R.J. Howerton, "Thresholds and Q Values of Nuclear Reactions Induced by Neutrons, Protons, Deuterons, Tritons, ^{3}He Ions, Alpha Particles, and Photons," UCRL-50400, Vol. 24 (March 1981).